BOLU ABANT IZZET BAYSAL UNIVERSITY
THE INSTITUTE OF GRADUATE STUDIES

INVESTIGATION OF UNIAXIAL AND BIAXIAL NEMATIC PHASE PROPERTIES OF DYE-DOPED LYOTROPIC LIQUID CRYSTALS

MASTER OF SCIENCE

GÖKHAN TOPÇU

BOLU, OCTOBER 2020

BOLU ABANT IZZET BAYSAL UNIVERSITY
THE INSTITUTE OF GRADUATE STUDIES
DEPARTMENT OF CHEMISTRY

INVESTIGATION OF UNIAXIAL AND BIAXIAL NEMATIC PHASE PROPERTIES OF DYE-DOPED LYOTROPIC LIQUID CRYSTALS

MASTER OF SCIENCE

GÖKHAN TOPÇU

BOLU, OCTOBER 2020

APPROVAL OF THE THESIS

INVESTIGATION OF UNIAXIAL AND BIAXIAL NEMATIC PHASE PROPERTIES OF DYE-DOPED LYOTROPIC LIQUID CRYSTALS submitted by **GÖKHAN TOPÇU** and defended before the below named jury in partial fulfillment of the requirements for the degree of **Master of Science** in **Department of Chemistry, Institute of Graduate Studies of Bolu Abant Izzet Baysal University in 22.10.2020** by

Examining Committee Members	**Signature**
Supervisor Assoc. Prof. Dr. Erol AKPINAR Bolu Abant Izzet Baysal University	....
Member Assoc. Prof. Dr. Abdulkadir ALLI Düzce University	....
Member Assist. Prof. Dr. Erhan BUDAK Bolu Abant Izzet Baysal University	....

Prof. Dr. Osman GÖRÜR **………………………………**

Director of Institute of Graduate Studies

To my family

DECLARATION

I hereby declare that all information in this document has been obtained and presented in accordance with academic rules and ethical conduct. I also declare that, as required by these rules and conduct, I have fully cited and referenced all material and results that are not original to this work.

Gökhan TOPÇU

ABSTRACT

INVESTIGATION OF UNIAXIAL AND BIAXIAL NEMATIC PHASE PROPERTIES OF DYE-DOPED LYOTROPIC LIQUID CRYSTALS
MSC THESIS
GÖKHAN TOPÇU
BOLU ABANT IZZET BAYSAL UNIVERSITY INSTITUTE OF GRADUATE STUDIES
DEPARTMENT OF CHEMISTRY
(SUPERVISOR: ASSOC. PROF. DR. EROL AKPINAR)

BOLU, OCTOBER 2020

In this study, the effects of the anionic azo dye Sunset Yellow on the stabilization of lyotropic uniaxial and biaxial nematic phases and the uniaxial to biaxial phase transitions were investigated. The dye was added in different concentrations to the host ternary mixture of cationic surfactant dodecyltrimethylammonium bromide, 1-dodecanol, and water. Furthermore, a comparative investigation was performed to examine the role of the dye in lyotropic mixtures by adding some inorganic salts to the same host mixture. Salts used for this purpose were NaBr, $NaNO_3$, $NaClO_3$, NaI, NaSCN, and $NaClO_4$. The lyotropic nematic liquid crystal properties of all the samples were investigated by polarizing optical microscopy, laser conoscopy, and small-angle X-ray scattering. The results indicated that (a) the anionic dye Sunset Yellow has a chaotropic character between that of the I^- and SCN^- ions, being similar to the second one, (b) it gives a larger biaxial nematic phase temperature range in the partial phase diagram in comparison with the SCN^- ion and other inorganic salts, and (c) it shifts the temperatures of both uniaxial to biaxial nematic phase transitions. The small-angle X-ray scattering results also indicated that, at least in the investigated concentration range, the dye is mainly located on the micelle surfaces, just like a conventional ion, and that on increasing concentration of the dye induces higher surfactant aggregation number in the micelles.

KEYWORDS: Lyotropic liquid crystal, Nematic phase, Biaxial nematic phase, Anionic azo dye sunset yellow, Surfactant-dye interactions, Polarizing optical microscopy, Laser conoscopy, Small-angle X-ray scattering.

ÖZET

BOYAR MADDE EKLENMİŞ LİYOTROPİK SIVI KRİSTALLERİN TEK EKSENLİ VE ÇİFT EKSENLİ NEMATİK FAZ ÖZELLİKLERİNİN İNCELENMESİ
YÜKSEK LISANS TEZI
GÖKHAN TOPÇU
BOLU ABANT İZZET BAYSAL ÜNİVERSİTESİ
LİSANSÜSTÜ EĞİTİM ENSTİTÜSÜ
KİMYA ANABİLİM DALI
(TEZ DANIŞMANI: DOÇ. DR. EROL AKPINAR)

BOLU, EKİM - 2020

Bu çalışmada, anyonik azo boyar madde olan Sunset Yellow'un lyotropik tek eksenli ve çift eksenli nematik fazların stabilizasyonu ile tek eksenli-çift eksenli faz geçişleri üzerindeki etkileri araştırıldı. Boyar madde farklı konsantrasyonlarda katyonik sürfaktant dodesiltrimetilamonyum bromür, 1-dodekanol ve su ana üçlü karışımına eklendi. Ayrıca, liyotropik karışımlarda boyar maddenin rolünü incelemek için aynı ana karışıma bazı inorganik tuzların eklenmesiyle karşılaştırmalı bir araştırma da yapılmıştır. Bu amaçla kullanılan tuzlar NaBr, $NaNO_3$, $NaClO_3$, NaI, NaSCN ve $NaClO_4$'tır. Tüm örnekler polarize optik mikroskopisi, lazer konoskopisi ve küçük açı X-ışını saçılması ile araştırılmıştır. Elde edilen sonuçlar anyonik boyar madde Sunset Yellow'un (a) I^- ve SCN^- iyonları arasında daha çok ikincisine yakın bir kaotropik karaktere sahip olduğunu, (b) SCN^- ve diğer anorganik tuz iyonlarıyla karşılaştırıldığında kısmi faz diyagramlarında daha geniş çift eksenli nematik faz sıcaklık aralığı verdiğini ve (c) her iki tek eksenli fazdan çift eksenli nematik faza geçiş sıcaklıklarını kaydırdığını (değiştirdiğini) göstermiştir. Küçük açı X-ışını saçılması sonuçları, en azından araştırılan konsantrasyon aralığında, boyar maddenin esas olarak geleneksel iyonlar gibi misel yüzeylerinde lokalize olduklarının ve artan boyar madde konsantrasyonuyla daha yüksek misel içinde sürfaktant kümelenme sayılarına sebep olduğunu da göstermiştir.

ANAHTAR KELİMELER: Liyotropik sıvı kristal, Nematik faz, Çift eksenli nematik faz, Anyonik azo boyar madde Sunset Yellow, Sürfaktant-boyar madde etkileşimleri, Polarize optik mikroskopisi, Lazer konoskopisi, Küçük açı X-ışını saçılması.

TABLE OF CONTENTS

Page

LIST OF FIGURES

Page

LIST OF TABLES

Page

LIST OF ABBREVIATIONS AND SYMBOLS

Ch_B	: Biaxial cholesteric phase
Ch_C	: Calamitic cholesteric phase
Ch_D	: Discotic cholesteric phase
cmc	: Critical micelle concentration
DDeOH	: 1-Dodecanol
DTMABr	**:** Dodecyltrimethylammpnium Bromide
$\vec{H}$	: Magnetic field direction
LCLCs	: Lyotropic chromonic liquid crystals
LLCs	: Lyotropic liquid crystals
LNPs	: Surfactant-based lyotropic nematic phases
M	: Columnar hexagonal
N	: Nematic phase
NaBr	: Sodium Bromide
$NaClO_3$	: Sodium Chlorate
$NaClO_4$	: Sodium Perchlorate
NaI	: Sodium Iodide
$NaNO_3$	: Sodium Nitrate
NaSCN	: Sodium Thiocyanate
N_B	: Biaxial nematic phase
N_C	: Calamitic nematic phase
N_D	: Discotic nematic phase
SSY	: Sunset Yellow
TLCs	: Thermotropic liquid crystals
X	: Mole fraction
χ	: Magnetic suspectibility
$\Delta n/\delta n$	: Birefringences
ΔT_{N_B}	**:** Biaxial Nematic Phase Range
$\Delta\chi$	: Diamagnetic susceptibility
°C	: Celcius Degree

ACKNOWLEDGEMENTS

Firstly, I would like to thank to my family for their endless support and endless sacrifices.

My deepest gratitude to my supervisor Assoc. Prof. Dr. Erol AKPINAR for their guidance, advice, criticism, encouragements and insight throughout the research.

I would also like to thank Assoc. Prof. Dr. Öznur DEMİR ORDU for her suggestions, referrers and comments.

I would like to also thank to The Scientific and Technological Research Council of TURKEY (TÜBİTAK, Grant no: 217Z079) for financial support to this study.

1. INTRODUCTION

Surfactants are amphiphilic molecules having a hydrophobic part that is a nonpolar hydrocarbon, fluorocarbon, or siloxane, and the hydrophilic part that is a polar part of a molecule (Neto and Salinas, 2005). At low surfactant concentrations, they align themselves side by side in the polar solvent medium at air-water or oil-water interface (Panizza et al., 2005). The hydrophobic parts of the surfactants exist in the air (or oil) while the hydrophilic ones are surrounded by water. When the concentration of the surfactant in the solution is increased, a supramolecular structure, so-called ‘micelle’ (Chakraborty and Moulik, 2005), is formed at critical micelle concentration (cmc) and micelles generally have spherical shape around the cmc. It is important to emphasize that micelles are the main structural unit of the two different systems which are called isotropic micellar solutions and anisotropic lyotropic liquid crystals. These two systems differ in terms of the preparation of samples. While isotropic micellar solutions can be prepared at low surfactant concentrations, on the contrary, lyotropic liquid crystalline phases are obtained at high surfactant concentrations, about 10^2 times of cmc (Neto and Salinas, 2005).

Both micellar systems may exhibit some similar properties. For instance, the addition of electrolyte screens the repulsions between the head groups on the micelle surfaces, which causes modifications on not only micelle size or shape but also the formation of different lyotropic structures. From this respect, the interactions between the surfactant head groups and the electrolyte ions or the surfactant counterions play a key role in the formation of different lyotropic liquid crystal phases.

Among the lyotropic liquid crystals, one of the common structures is the nematic phases. They have some biotechnological applications because of their well-known property that the micelles with their local directors tend to align with respect to a preferred direction. Some studies were performed in the literature to understand the formation mechanisms of different nematic phases, however, there still exist some controversies on those mechanisms. Considering the aim of the present thesis, it will be shown for the first time how surfactant-dye interactions on the micelle surfaces induce different lyotropic nematic phases. Furthermore, the effects of surfactant-dye interactions on uniaxial-to-biaxial phase transitions and the formation of wider biaxial nematic phase region in the partial phase diagrams will be revealed in the frame of this thesis with strong experimental evidences.

In the following parts, some important theory related to the liquid crystals is given before discussing the experimental results of the thesis.

1.1 Liquid Crystals

Liquid crystals were firstly noticed by Austrian plant botanist Friedrich Reinitzer and German physicist Otto Lehmann (1888) for some derivatives of cholesterol (Geelhaar et al., 2013). The discovery of this liquid crystal material caused a lot of inventions in the area of technology, biotechnology, industry, and pharmacology, etc (Neto and Salinas, 2005). The liquid crystals are accepted as a meta-state of matter between liquid and solid states and hence the term “mesophase” is also used to describe the liquid crystalline phases (Figure 1.1). They are also considered as the fourth state of matter and they can show some properties of both solid and liquid. For example, they have some degree of fluidity like a liquid, and, at the same time, their molecules may be oriented in a crystal-like way. Ordinary solids and liquids can be turned into each other as the temperature increases or decreases. In the solid state, the molecules have positional and orientational orders. However, the molecules lose both orders in the liquid state with free flow and random molecular motion. The liquid crystals possess, in general, no positional order but a certain degree of orientational orders, however, for some liquid crystal structures, it was reported that the molecules may have some degree of positional order (Neto and Salinas, 2005). From the positional and orientational orders point of view, the liquid crystal material may be more liquid like or solid-like. The degree of order is quantitatively characterized by the order parameter, S, which is given by the following equation (Senyuk, 2020)

$$S = \frac{1}{2}\langle 3cos^2\theta - 1\rangle \tag{1.1}$$

where θ is the average angle between the long axes of the molecules in the liquid crystal material and a certain axis or direction, so-called “phase director” or “optical axis”, along which the molecules tend to align (Figure 1.2). The brackets denote spatial average.

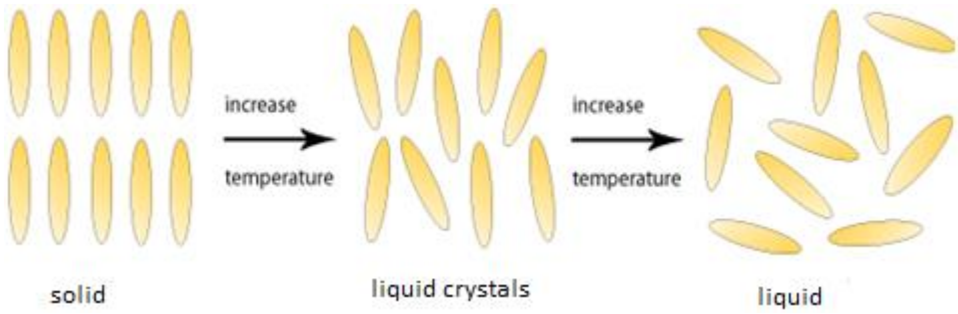

Figure 1.1. Representation of the molecular arrangement in three states of matter with the change in temperature (Ibrhim et al., 2017).

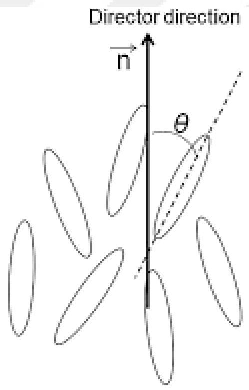

Figure 1.2. Local alignment of long axes of the molecules (Ishihara and Mizusaki, 2019).

The order parameter can take a value between 0 and 1. In the case of S=0, the molecules align in all directions in space. So, the average value of the term $\langle 3cos^2\theta - 1\rangle$ in the equation 1.1 is zero and the material is called an isotropic liquid. If the S=1, all molecules align parallel to the director, θ=0°, which is seen in a perfect crystal (solid). In other words, while there exists a completely random molecular order in the isotropic liquid, the molecules are perfectly aligned in the perfect crystal. Generally, the order parameter takes a value of about 0.3-0.8 for a liquid crystal sample and it decreases with temperature (Senyuk, 2020). A sharp decrease in the order parameter is observed at a specific temperature, so-called “critical transition temperature, T_c”, at which a phase transition from a liquid crystal phase to an isotropic liquid phase occurs (Figure 1.3).

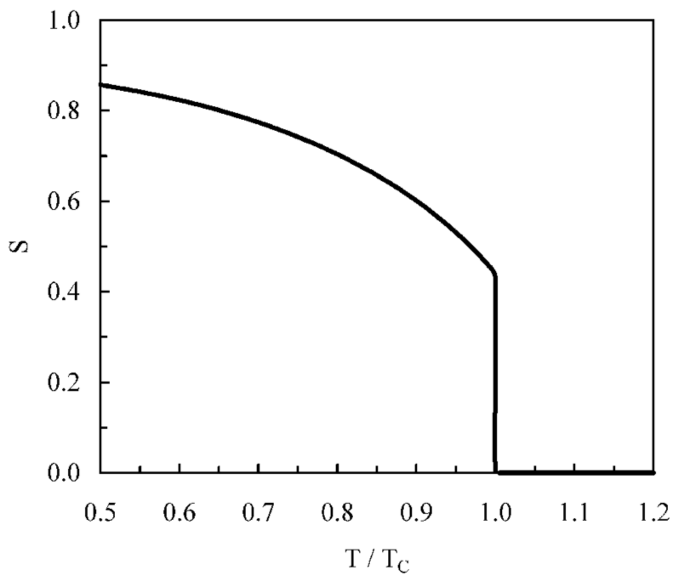

Figure 1.3. Order parameter as a function of temperature (Gennes, 1974).

Two main types of liquid crystals are defined: *thermotropic* (TLCs) and *lyotropic* (LLCs) liquid crystals. LLCs are generated with interactions between anisotropic aggregation of surfactant molecules in fluid anisotropy, and the formation of different LLC structures depends on both (a) *the relative concentration of constituents in the solution* and (b) *temperature* (Singh, 2002), while TLCs have arisen with interactions among partially rigid anisotropic molecules in orientational order and only a function of *temperature*. For both types of liquid crystals, the temperature is an important driving force for obtaining different mesophase structures. If the temperature is increased extremely, the delicate cooperative ordering of the LC phase is suffered from thermal motion and the material goes into the conventional isotropic liquid phase (Birdi, 2014). If the temperature is too low, most materials transform into the conventional crystal. Their molecular structures are represented by 'rigid rods' which is quite complicated. These rigid rods form the distinctive ordered structure by interacting with one another. TLCs can be seen in many variations of phases depending on the changing of the temperature. TLCs have three main phases as nematic, cholesteric, and smectic but TLCs are not the main subject of this thesis, therefore, this issue will not be discussed further. LLCs and their properties will be discussed in detail in the next parts.

1.1.1 Lyotropic Liquid Crystals

LLCs are in close contact with biology and the understanding of their physicochemical properties plays an extremely important role in some technological/biotechnological applications such as soap, pharmacy, cosmetics, food, etc. (Neto and Salinas, 2005). They are obtained by dissolution of amphiphilic or surfactant molecule in a suitable polar solvent (mostly water). The surfactant molecule consists of two parts: water-miscible hydrophilic and immiscible hydrophobic parts, Figure 1.4 (Fairhurst et al., 1998). When these compounds are dissolved in water, they spontaneously self-assemble to produce supramolecular structure “micelle” at a certain surfactant concentration (Figure 1.5). This concentration is called “cmc” and each surfactant has a specific cmc value.

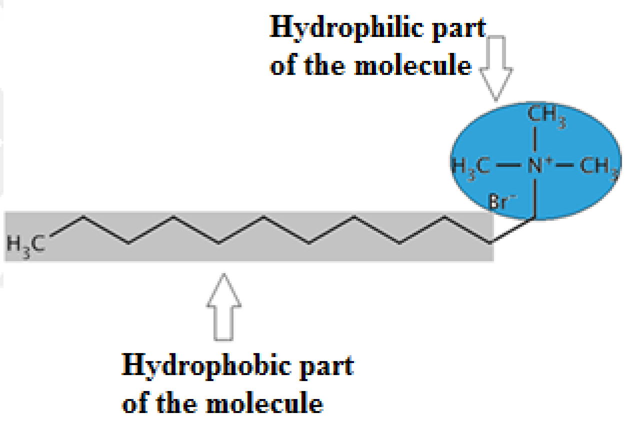

Figure 1.4. Representation of the hydrophilic and hydrophobic parts of the surfactant molecule, for instance, dodecyltrimethylammonium bromide.

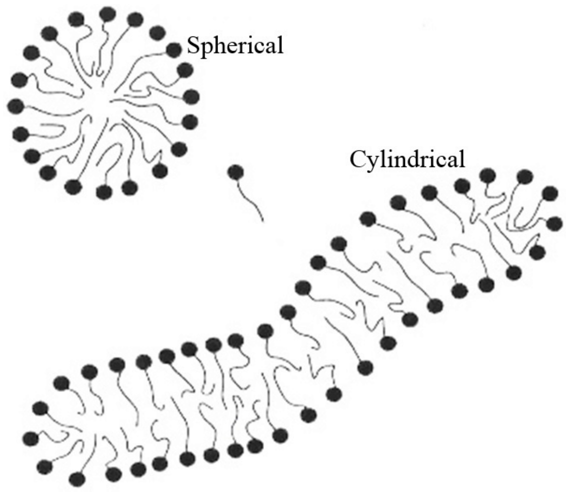

Figure 1.5. Representation of spherical and cylindrical micelles (Oliveira, 2006).

The micelles are spherical and consequently not anisotropic around cmc. When the concentration of surfactant molecules is high enough (about ~10^2.cmc) at a suitable temperature, LLCs are obtained by forming micelles of small shape anisotropy. For instance, potassium laurate/water mixture, cmc= 0.024 moles/kg (Kale and Zana, 1977) and liquid crystalline phases are c_{surf} > 2 M (Lenglet et al., 2002). Temperature and concentration of the surfactant are so important in LLCs for obtaining different mesophases. The importance of these parameters can easily be seen in the graph of temperature versus amphiphile concentration (Figure 1.6). Krafft temperature is defined as the point at which amphiphile starts to be dissolved in a solvent and below this temperature, no micelles exist in the solution (Heakal and Elkholy, 2017). When we look at the left side of the graph, we can easily see free amphiphiles. As the temperature and concentration of the amphiphile increase, various phases of the LLCs are formed. At any point in the concentration, after the system reaches the crystal state, there is an intermediate gel phase (Neto and Salinas, 2005). This phase is normally stable if the temperature does not decrease extremely. If it does, it goes spontaneously towards the crystalline phase. (Neto and Salinas, 2005).

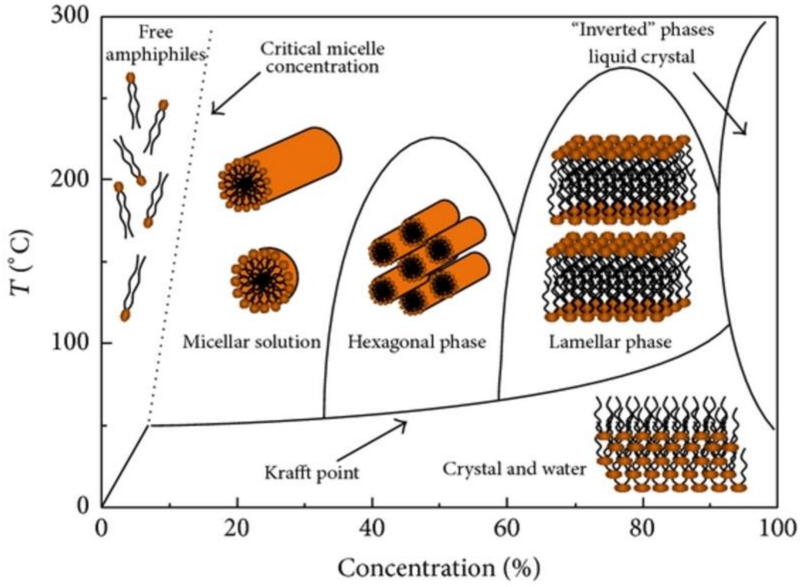

Figure 1.6. A typical phase diagram for lyotropic liquid crystals obtained from the dissolution of surfactants in a selective solvent (Lombardo et al., 2015)

Some parameters affect the formation of different types of lyotropic structures such as the ionic character of the polar head of the surfactant molecule, the concentration and structure of cosurfactant, the pH and ionic strength of the solution, purity of the compounds, the existence of electrolyte, etc.

1.1.1.1 Lyotropic liquid crystalline structures

Lyotropic liquid crystals are one of most of the richest examples in terms of polymorphism. They are divided into five main categories according to their various property such as structural shape, birefringences, symmetry axes, dimensional ordering (Bilinov, 2011; Burducea, 2004). These are hexagonal, lamellar, nematic, cubic, and cholesteric (chiral nematic) phases. In the frame of the thesis, the main subject is nematic phases, but brief information will give about other structures of the lyotropic liquid crystals.

In the lamellar phase, surfactant molecules present at relatively higher concentrations and form bilayers separated by water layers with a large shape anisotropy in one direction (Figure 1.7). The thickness of the layers is up to the length of the two main surfactant molecules (but the single-layered structure can be observed in some cases) (Neto and Salinas, 2005). The thickness of the bilayers depends on the polarity of the solvent and temperature of the sample.

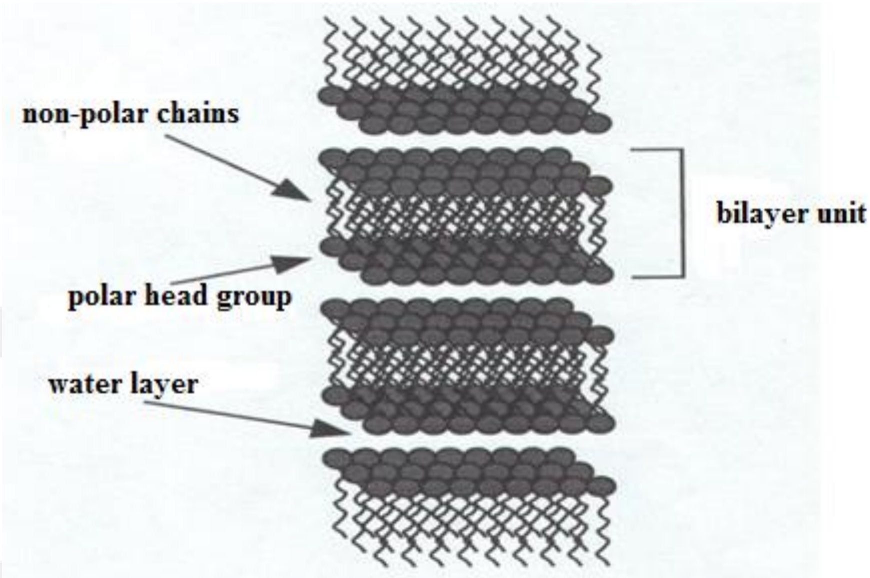

Figure 1.7. Representation of aggregation of the surfactant molecules in the bilayers of the lamellar phase.

The lamellar phase is commonly present in organisms (Garti and Aserin, 2012). It is basically characterized in two ways as L_α and L_β. The L_α is observed at very high surfactant concentration and differs from the other one due to properties of having liquid-like state, and flat view. This phase is also called "neat soap" (Lenglet et al., 2002). The main property that separates L_β from L_α is the state of the carbonic chains of the surfactants. L_β phase is stiff and has solid-like ordered hydrocarbon chains which are packed in a two dimensional and exhibit all-trans conformations. This phase is also called the "gel" phase (Alfutimie et al., 2014).

In the hexagonal phase, cylindrical micelles are constructed by surfactant molecules with a large shape anisotropy. The diameter of the cylinders is up to the length of the two main surfactant molecules and the length of the cylinders is larger than its diameter about 50 times (Neto and Salinas, 2005). Parallel cylinders are disposed of a hexagonal lattice and perpendicular to axes in the plane. There are two different structures in the hexagonal phase as a direct and inverted structure (Neto and Salinas, 2005). Direct structures are prepared by using polar solvent and they display liquid-like ordering. This phase is also called "middle soap" and denoted H_I or H_α or E (Lenglet et al., 2002). In contrast to direct structure, an inverted structure presents with a large concentration of the nonpolar solvents (Neto and Salinas, 2005). The aggregation of polar and nonpolar groups is exactly opposite of the direct structure. This phase is denoted F or H_2 (Lenglet et al., 2002). There are examples of the direct and inverted structures in Figure 1.8.

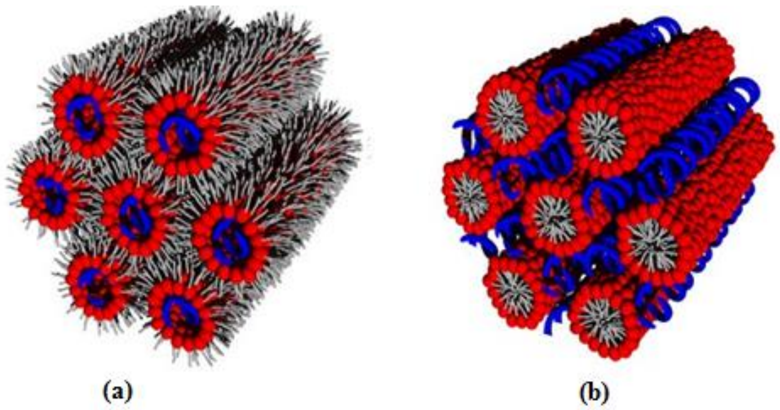

Figure 1.8. Representation of (a) inverted and (b) direct structures of the hexagonal phases of the lyotropic liquid crystals. (Tresset, 2009).

In the cubic phase, surfactant molecules aggregate in the form of spherical micelles and have three-dimensional repeating order (Lombardo et al., 2015). Two arrangements are available in this phase as cubic centered and bicontinuous arrangements (Rizwan et al., 2010). Space between repeating units is filled by water molecules similar to the lamellar phase. Lyotropic cubic phases are also known as "viscous isotropic phases" (Fontell, 1990) because they display isotropic property unlike other phases of the lyotropic liquid crystals. Distinguishing property of the lyotropic cubic phases from other lyotropic ones is their very high viscosities. They can be observed as dark and featureless under a polarizing optical microscope. Hexagonal and cubic phases are used in the drug delivery systems as a solubilizing component of the drug in blood and take a strong role to release and transfer drugs towards living metabolism systems (Chen et al., 2014; Shah et al., 2001; Chang and Bodmeier, 1997; Fong et al., 2016).

Cholesteric phases arise from the existence of a chiral dopant molecule in a lyotropic mixture (Kroin and Neto, 1987; Fontaini et al., 1996). Adding any chiral molecule to the mixture that gives a nematic phase is already enough for obtaining a cholesteric phase if the concentration of the chiral dopant is greater than the critical concentration. They are named in two ways according to preparation. The first one is the intrinsic cholesteric phase which is obtained by using chiral amphiphilic/surfactant molecule as a main surfactant molecule of the mixture (e.g. potassium N-dodecanoyl-L-alaninate (Akpinar et al., 2013)) (Neto and Salinas, 2005). The second one is the extrinsic cholesteric phase which is obtained by adding a non-amphiphilic chiral molecule (e.g. brucine sulfate (Akpinar et al., 2018b)) to the mixture (Neto and salinas, 2005). There are three types of cholesteric phases as discotic (Ch_D), calamitic (Ch_C) and biaxial (Ch_B) (Fontaini et al., 1996) (Kroin and Neto, 1987) (Nehring and Saupe, 1972). It is reported that the concentration of chiral molecules must be at least 0.05 M % in the sample to obtain a cholesteric structure (Neto and Salinas, 2005). Cholesterics form helical structure and they have the helix axis that is optical director of the cholesteric phases. They are characterized by the polarizing optical microscopy with their characteristic fingerprint or spaghetti-like textures (Figure 1.9).

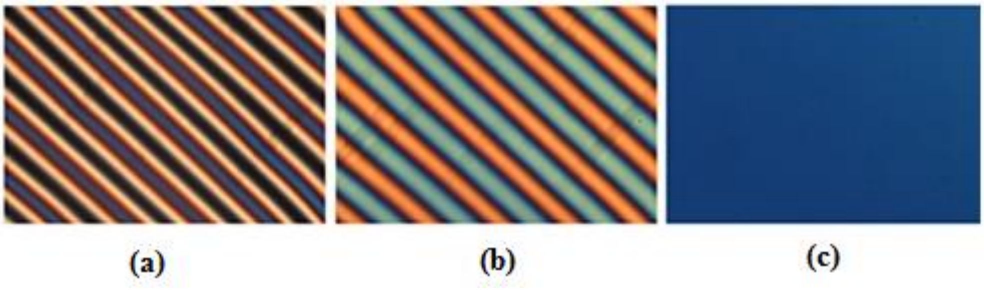

Figure 1.9. Magnetically well-aligned lyotropic cholesteric (a) discotic, (b) biaxial and (c) calamitic textures (Akpinar et al., 2019a)

In the case of the uniaxial Ch_D phase, there are dark (black) regions between the cholesteric lines (for example, Figure 1.9a). In fact, these regions correspond to the homeotropic alignment of the local optical axes of the micelles along the z-axis direction, which is parallel to the incoming light propagation direction (Figure 1.10). In the homeotropic regions, the local optical axes of the micelles (m) is parallel to the light coming under polarized optical microscope, but perpendicular to both the magnetic field and the helix axis directions. In the Ch_D phase, the local director is oriented perpendicular to the helix axis but also rotates around this axis. When the Ch_D-Ch_B phase transition occurs, homeotropic regions between cholesteric lines are no longer observed because the system has two optical axes rotating along a plane in the direction of the magnetic field and around the helix axis (Figure 1.9b) (Neto and Salinas, 2005; Neto, 2014). The angle (θ) between these two optical axes has a rather small value in the vicinity of Ch_D-Ch_B phase transition, and this angle grows within the Ch_B region. When temperature is changed more, the Ch_C phase is now stabilized and $\theta = \pi$. In the uniaxial Ch_C phase, the helix structure is lost due to the local director of the micelles parallel to the magnetic field and helix axis direction, that is, no cholesteric line is observed (Figure 1.9c). How the local optical axes are oriented in all three cholesteric phases is summarized in Figure 1.11 (Neto, 2014).

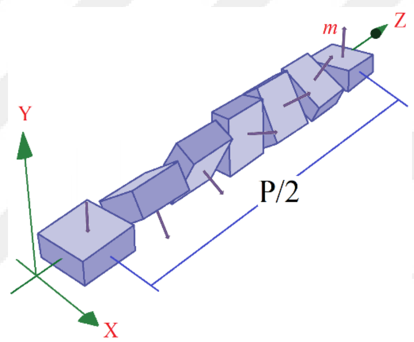

Figure 1.10. Representation of the organization of the orthorhombic micelles (Neto et al., 1985) with their local directors (m) along the helix axis, which is in the direction of the z-axis.

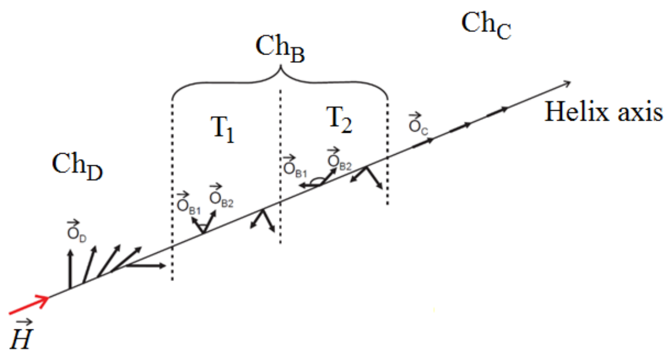

Figure 1.11. Orientation of local optical axes (indicated by a black arrow) in all three nematic phases in the presence of a magnetic field, $\vec{H}$ (Neto, 2014). $\vec{O}_D$, $\vec{O}_B$ ($\vec{O}_{B1}$, $\vec{O}_{B2}$) and $\vec{O}_C$ show local optical axes in the Ch_D, Ch_B and Ch_C phases, respectively.

Another lyotropic structure is nematic phases and there are several studies reported in the literature to investigate their physicochemical properties. They are also subject to this thesis, thus a detailed information about them can be found below.

1.1.1.2 Lyotropic Nematic Phases

Lyotropic nematic phases were firstly reported by Lawson and Flautt for a mixture sodium decyl sulfate/sodium sulfate/decanol/water (Lawson and Flautt, 1967). Three types of lyotropic nematic phases are available as N_D (discotic) and N_C (calamitic) phases, which display uniaxial character (Berejnov et al., 1998; Galerne et al., 1987), and N_B (biaxial) phase (Galerne et al., 1987; Oliveira et al., 1996). Uniaxial systems are identified by exhibiting preferential orientation of their phase directors with respect to applied external magnetic field direction (Boden et al., 1981). The decisive factor of the director orientation for the nematic phases is diamagnetic susceptibility anisotropy of alkyl chains of the surfactant molecules, $\Delta\chi = \chi_{//} - \chi_{\perp}$, where // and $\perp$ represent the alignment of the nematic phase's director in parallel and perpendicular directions, respectively, to the applied magnetic field (Boden et al., 1981). If $\Delta\chi<0$ ($\chi_{//} < \chi_{\perp}$), the director of the nematic phase aligns perpendicular to the magnetic field direction and this is seen in the N_D phase (Figure 1.12a). If $\Delta\chi>0$ ($\chi_{//}>\chi_{\perp}$), which means that the director of a phase aligns parallel to the magnetic field direction, this indicates the N_C phase (Figure 1.12b).

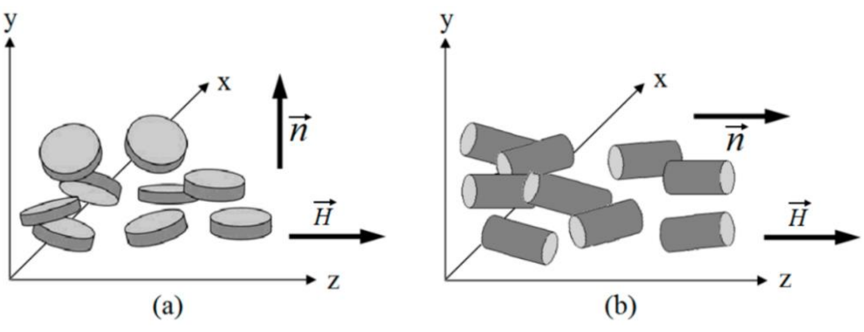

Figure 1.12. Alignment of the nematic phase director, $\vec{n}$, in (a) the N_D and (b) the N_C phases. According to the early studies on the nematic phases, it was assumed that the N_D and N_C phases were composed of disc-like and cylindrical-like micelles, respectively. $\vec{H}$: magnetic field direction.

Unlike the uniaxial nematic phases, there are three diamagnetic susceptibilities along their respective two-fold symmetry axes or directors for the biaxial nematic phases: χ_{ii}, where i=1, 2 and 3 (Luckhurst and Sluckin, 2015). Then, the diamagnetic susceptibility anisotropy is given by

$$\Delta\chi = \chi_{33} - \frac{\chi_{11} + \chi_{22}}{2} \tag{1.2}$$

for the lyotropic biaxial nematic phases. Two different $\Delta\chi$ are possible being as $\Delta\chi>0$ or $\Delta\chi<0$. In the former (latter) case, the largest (smallest) diamagnetic susceptibility is greater (smaller) than the average of the diamagnetic susceptibilites of other axes and the biaxial phase aligns parallel (perpendicular) to the magnetic field direction (Quist, 1995; Filho et al., 2003). Thus, from the alignment property of the biaxial phase point of view, the presence of the external magnetic field causes the classification of two different biaxial nematic phases, N_B^+ and N_B^-. However, they thermodynamically belong to same and unique biaxial nematic phase, i.e. they are not a distinct phase from one another.

Liquid crystals, of course lyotropic nematics, are anisotropic materials. When a polarized light beam is sent to those kind of materials, two rays are produced being as ordinary and extraordinary rays. They pass through the liquid crystal sample with different velocities and this causes two different refractive indices, n_o and n_e, respectively. Furthermore, the vibration direction of the electric vectors of the ordinary and extraordinary rays may be perpendicular or parallel to the optical axis of the nematic phase. It is known that the electric vector of the ordinary (extraordinary) ray is perpendicular (parallel) to the optical axis, n_o (n_e), and $n_o=n_\perp$ and $n_e=n_{//}$. The difference between these two refractive indices gives double refraction or birefringence, $\Delta n=n_e-n_o=n_{//}-n_\perp$. Similar to the definition of the diamagnetic susceptibility anisotropy, the Δn may take values greater than zero ($n_{//}>n_\perp$) or smaller than ($n_{//}<n_\perp$). Thus, in the case of the lyotropic nematic phase, two different nematic phases are described with positive and negative birefringences. If the diamagnetic susceptibility anisotropy is compared with the birefringence, the former has opposite sign with respect to the latter, i.e., for instance, $\Delta\chi<0$ and $\Delta n>0$ for the N_D phase, and $\Delta\chi>0$ and $\Delta n<0$ for the N_C phase.

In addition to the $\Delta\chi$ and Δn for the characterization or classification of the lyotropic nematic phases, the micelle shape is another criterion. In early studies, it was assumed that the micelles have disc- or cylindrical-like shape, as shown in the Figure 1.12., for the N_D and N_C phases, respectively. However, this was only an assumption because there were no strong experimental evidences to support the existence of those types of the micelles in the lyotropic nematic phases. After reporting first lyotropic nematic phase in the literature, Freiser theoretically predicted for the first time that the micelles may have biaxial symmetry in the nematic phases by considering the interaction energy and the orientations of two non-symmetric molecules (Freiser, 1970, 1971). The Freiser's prediction was experimentally realized in 1980 by finding the first lyotropic mixture, potassium laurate (KL)/decanol (DeOH)/D_2O, exhibiting biaxial nematic phase in addition to the uniaxial ones (Yu and Saupe, 1980).

After the discovery of the lyotropic biaxial nematic phase, several studies were conducted to understand the formation mechanisms of the lyotropic nematic phases (Akpinar and Neto, 2019). Those studies were mostly concentrated on whether the biaxial nematic phase is a thermodynamically stable phase or a consequence of the coexistence of other two uniaxial nematic phases (N_D and N_C). Later, studies in the following years revealed with strong experimental findings such as conoscopic investigations by polarizing optical microscopy, small-angle x-ray scattering and laser conoscopy showed that the biaxial nematic phase is a thermodynamically stable (Akpinar et al., 2012b)

Some models were proposed for the formation mechanism of the nematic phases. A reliable and an important one was suggested by Neto (Neto et al., 1985) and Galerne (Galerne et al., 1987), for the N_B phases by rejecting the idea of the coexistence of two uniaxial phases. They carried out some X-ray diffraction studies on the mixture KL/DeOH/D_2O and showed that the micelles are built up of biaxial platelets or pseudo-lamellar structure in all three nematic phases. It means that three nematic phases consist of micelles with similar shape. Their model is called "intrinsically biaxial micelles, IBM, model", and it mainly assumes two parameters: (a) micelle symmetry and (b) orientational fluctuations. According to the IBM model, the micelles have orthorhombic symmetry (Figure 1.13a), with typical dimensions A′, B′ and C′, and α, β and γ may be chosen as the axes of the coordinate system, fixed in the micelles. The orthorhombic micelles exhibit different "orientational fluctuations" to give N_D, N_B or N_C phases. The orientational fluctuations around the axis 3 perpendicular to the largest micelle surface (along the symmetry axis γ) give rise to the formation of the N_D phase (Figure 1.13b), with the micelle size A'~ B'. The small amplitude orientational fluctuations along three axes (1, 2 and 3) lead to the formation of the N_B phase. The orientational fluctuations around the long micellar axis (parallel to the axis 1 and along the symmetry axis α), the N_C phase is now obtained (Figure 1.13c).

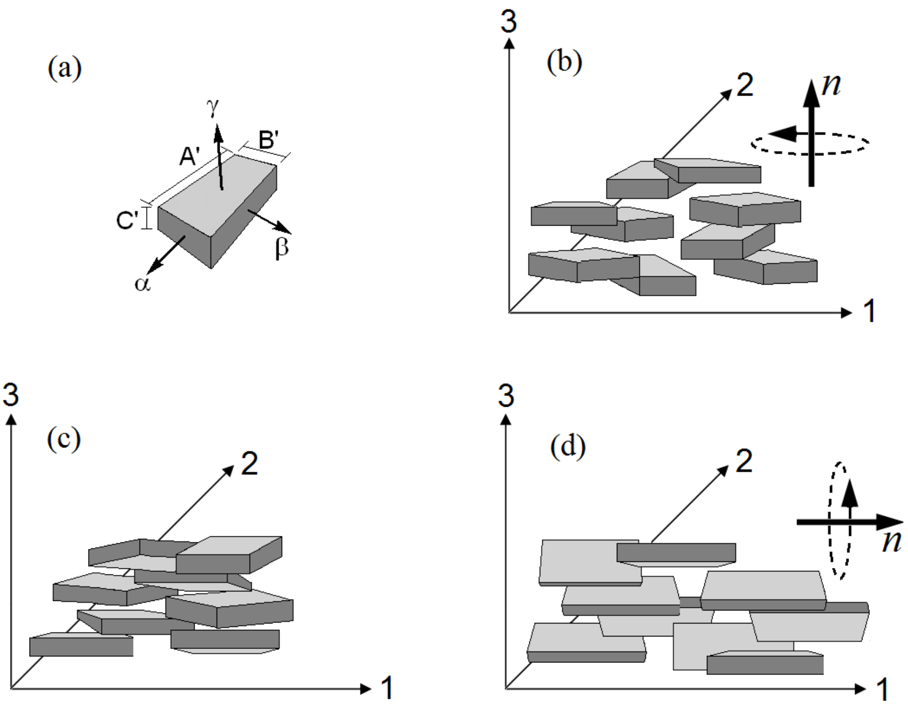

Figure 1.13. (a) Sketch of the orthorhombic micelle in the framework of the IBM model. The detergent amphiphilic bilayer is represented by C'. (b) N_D phase (c) N_B phase and (d) N_C phase (Akpinar and Neto, 2019).

Unlike the early studies, the factors that affect the formation of the nematic phases, especially biaxial one, have been reported in the recent studies from the lyotropic mixture preparation point of view. For instance, it was shown that relative alkyl chain lengths of both (a) surfactants (Akpinar et al., 2018a) and (b) long chain alcohols (Akpinar et al., 2012b) play very important roles on the formation of the nematic phases. Furthermore, (c) kosmotrope and chaotrope properties of counterions and ions (Akpinar et al., 2016a), and (d) localization of dopant molecules on the micelle surfaces (Akpinar et al., 2016b) are important factors on the stabilization of different nematic phases. The studies of Refs. (Akpinar et al., 2012a; Oliveira et al., 1989) indicated that a molecular segregation between the surfactant and the co-surfactant (i.e., long chain alcohols) in the micelles should occur to obtain the N_B phase region in the partial phase diagrams, and there is a relationship between the alkyl chain length of alcohol (n_{alc}) and main surfactant (n_{Surf}) molecules: $n_{alc} = n_{Surf} \pm 2$ (Akpinar et al., 2012a) (Figure 1.14).

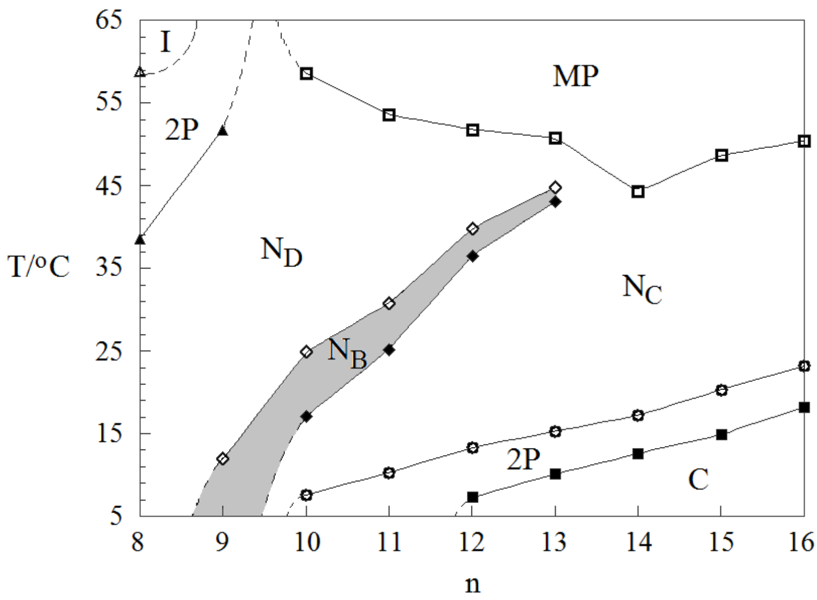

Figure 1.14. Partial phase diagram of KL/K_2SO_4/alcohol/water mixtures (Akpinar et al., 2012a). n is the number of carbon atoms in the alkyl chain of the alcohol molecules. I, 2P, MP and C represent an isotropic phase, two-phase region, multi-phase region and crystalline-like phase.

1.1.1.3 Lyotropic Chromonic Liquid Crystals

Another sub-class of the lyotropic liquid crystals is "Lyotropic chromonic liquid crystals (LCLCs)", which are obtained from the binary aqueous solutions of dye (Lydon, 2004) or drug (Collings et al., 2016) molecules. Those kinds of molecules have multi-aromatic rings, polar substituents, and ionic groups. Structural units of LCLCs are stacks of noncovalent molecules which are the process of reversible self-assembly on top of each other in aqueous solution. This is also called

"H aggregates" (Tam-Chang and Huang, 2008; Lydon, 2010). The molecules in the LCLCs have a central core that has a plank-like or disk-like polyaromatic parts with polar groups at the periphery (Tam-Chang and Huang, 2008). When the concentration of stacks (aggregates) is high, they form mesophase by ordering regularly (Edwards et al., 2008; Tidy et al., 1995). There are two chromonic mesophases, known as uniaxial nematic (N) and the columnar hexagonal (C or M) phase (Figure 1.15) (Tam-Chang and Huang, 2008; Lydon, 2010). The first study of LCLCs came from Alfred Saupe and L.J. Yu in 1982. They investigated the stability of the nematic phases obtained from a drug molecule, disodium cromoglycate (DSCG), by using deuteron magnetic resonance spectroscopy (Yu and Saupe, 1982).

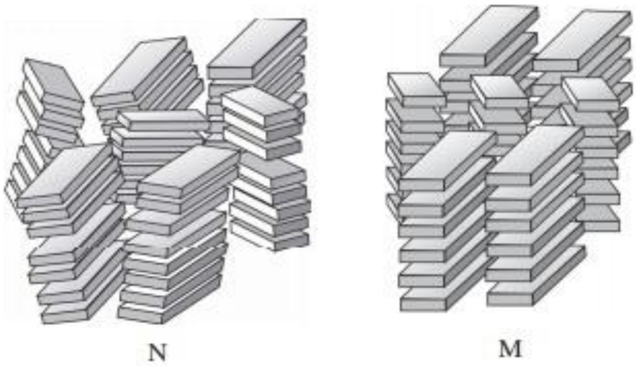

Figure 1.15. Stacks of the molecules in lyotropic chromonic N and M phases.

As seen in Figure 1.15, while the molecules aggregate by stacking in columns with no positional order in a nematic array, however, in the M phase, the columns are in a hexagonal array (Lydon, 2011). The molecules have a short-range arrangement of 150-700 Å in layer planes. The hexagonal packing spreads out to long distances while the positional ordering has a short-range. The hexagonal packing matrix, which has the same direction both in the plane and between the planes of the layers, can extend in three dimensions. The ordering has an orientation of the hexagonal packing array, which extends to infinity in three dimensions in the well-aligned system, and is called long-range bond orientational order (Halperin and Nelson, 1978).

One of the most common dye molecules to obtain LCLC is “Edicol Sunset Yellow”. It is a food colorizing azo dye that gives both nematic and hexagonal forms in water depending on the concentration. The phase diagram and the polarizing optical microscope textures of the sunset yellow/water system are given in Figure 1.16 (Park et al., 2008).

(a)

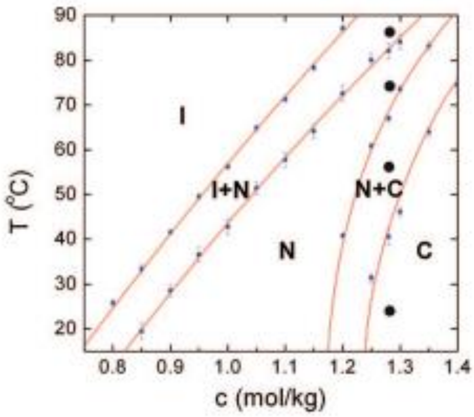

(b)

Figure 1.16. (a) Phase diagram of the SSY/water system and (b) polarizing optical microscope textures (Park et al., 2008).

1.2.2 Dye-Surfactant Interactions

The interactions between dye and surfactant molecules in dilute solutions have been widely used in various dyeing processes due to their practical importance and applications like photography, textile dyeing, hair coloring, etc (Fazeli et al., 2012). Knowledge of dye surfactant interactions has been helped to understand chemical equilibria, fluorescence reactions, mechanism and kinetics of the reaction between surfactant and sensitized color (Gokturk and Tuncay, 2003a). Many various parameters can affect the interactions between dye and surfactant molecules such as the charge and the alkyl tail length of the surfactants, and the type and the position of the substituents in the aromatic ring of the dye molecules (Tunc and Duman, 2007). In surfactant-dye interactions, surfactants that are used in the solution may be conventional or gemini (Fazeli et al., 2012). As mentioned in previous sections, surfactants are molecules that include both hydrophobic and hydrophilic parts in their structure. On the other hand, gemini surfactants are the molecules that contain two surfactant alkyl chains in which their heads are chemically bonded to each other by a spacer (Kirby et al., 2003). In the contrary to other surfactants, gemini surfactants display different properties such as much lower critical micelle concentration, higher surface activity, better dispersing, wetting, and solubilizing properties (Sohrabi et al., 2010; Jennings et al., 2002). The addition of small amounts of surfactant can change the solution properties of dye solutions such as electrical conductivity and absorption spectrum (Yang, 2004). These changes are a function of surfactant concentration in the measured quantities and indicate a small variation in the solution (Yang, 2004). Dye-surfactant complex in the solution is formed by the attractive forces between the dye and surfactant molecules when the charge of the dye molecule is contrary to the charge of the surfactant (Simoncic and Kovac, 1998). There are mainly many reasons for the formation of dye-surfactant aggregates in oppositely charged dye-surfactant interactions such as the formation of dye-surfactant salts, ion-pairs, the existence of ion-association complexes between ionic surfactants and dyes, and self-aggregation of dye (Gokturk and Tuncay, 2003b; Gohain and Dutta, 2008). Many noncovalent interactions (electrostatic, hydrophobic, hydrogen-bond and pep stacking interactions) help to organize the aggregations with the attachment of dye molecules to surfactants (Zhang et al., 2007).

In this thesis, Sunset Yellow was used to investigate dye-surfactant interactions and its behavior in the lyotropic nematic liquid crystals. Sunset Yellow (sodium (E)-6-hydroxy-5-((4-sulfonatophenyl) diazenyl naphthalene-2-sulfonate) (shown in Figure 1.17) is a dye molecule that is also dianionic monoazo dye compound and already used to form lyotropic liquid crystal phases depending on composition and temperature (Renshaw and Day, 2010). It is used to obtain red or yellow color in different industry, and it is also used in foods (Almeida et al., 2010). Sunset Yellow has two sulfonate groups at either end of the molecule and becomes well soluble in aqueous solution (Fazeli et al., 2012). In the forming of dye aggregates (H-aggregates rather than J-aggregates), this compound has more affinity because of the azo-hydrazone tautomerism as reported by pep stacking interactions between the aromatic rings in aqueous solution (Nehalatha et al., 2008; Chami and Wilson, 2010)

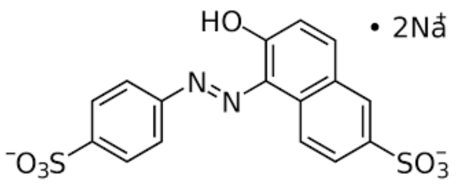

Figure 1.17. Molecular structure of Sunset Yellow.

2. AIM AND SCOPE OF THE STUDY

Surfactant-based lyotropic nematic phases (LNPs) and their phase diagrams as a function of concentration and/or temperature have been investigated in a wide range of studies (Boden et al., 1987; Oliveira et al., 1989; Ho et al., 1981; Nicolettat et al., 1991; Filho et al., 2003; Akpinar et al., 2012a; Wolff and Klaussner, 1995). In general, the mixtures presenting the LNPs are obtained by the dissolution of surfactant molecules in water. In most cases, electrolytes and/or cosurfactants are added to those solutions (Vasilevskaya et al., 1990; Braga et al., 2007; Simoes et al., 2010; Akpinar et al., 2012b; Akpinar et al., 2016a). Considering the symmetry of the LNPs, they are classified as uniaxial (discotic, N_D, and calamitic, N_C) with $D_{\infty h}$ symmetry and biaxial (N_B) with D_{2h} symmetry (Madsen et al., 2004; Akpinar and Neto, 2019). The main characteristic of those uniaxial phases is that the local symmetry axis of their structural units, micelles, exhibits an average alignment along a preferred direction (optical axis or director, $\vec{n}$). While only one optical axis exists in the N_D and N_C phases, the N_B phase has two optical axes and three orthogonal two-fold symmetry axes ($\vec{l}$, $\vec{m}$ and $\vec{n}$, where $\vec{n} = \vec{l} x \vec{m}$) (Nasrin et al., 2016; Kim et al., 2014; Kim et al., 2016). Another important point for the LNPs is that the N_B phase is mainly located between the other two uniaxial phases in the phase diagrams of lyotropic mixtures presenting the three nematic phases (Yu and Saupe, 1980; Bartolino et al., 1982; Akpinar et al., 2019b). As theoretically predicted by a Landau-type mean-field theory and experimentally verified, the uniaxial to biaxial transition is of second-order (Yu and Saupe, 1980; Bartolino et al., 1982; Akpinar et al., 2019b; Freiser, 1970; Alben, 1973).

Not only in surfactant-based LNPs but also in lyotropic chromonic nematic phases (LCNPs), some aspects about the stabilization mechanism of those phases have been investigated. For instance, Kumar et al. studied the effect of dye concentration, temperature, and ionic additives from the inter- and intra-aggregate spacings change point of view via x-ray diffraction and polarizing microscopy (Joshi et al., 2009). However, the surfactant-based LNPs were more investigated if compared with LCNPs. Especially, after the discovery of the first lyotropic mixture presenting the biaxial nematic phase (Yu and Saupe, 1980), numerous studies have been performed for characterization of properties and structures of both uniaxial and biaxial LNPs. Researchers worked to understand the aspects that affect the stabilization of different nematic phases. Among them, it was shown that the interactions between ionic species (the ionic head group of the surfactants and counterions and/or ions of the electrolytes) at the micelle surfaces play a key role in the stabilization of different LNPs (Akpinar et al., 2016a).

The surfactant-dye interactions have been studied for some dye/surfactant dilute-aqueous solutions because such interactions are important for both industrial and biotechnological applications (Fazeli et al., 2012; Buwalda and Engberts, 2001; Gokturk and Tuncay, 2003b; Khan and Sarwar, 2006; Shahir et al., 2011; Erdinc and Gokturk, 2014). However, the effect of those interactions on the stabilization of uniaxial and biaxial LNPs has not been investigated. In the present study, we combine molecules that, in water, present chromonic lyotropic mesophases with usual micellar lyotropic mixtures to stabilize the three nematic mesophases. We chose a cationic surfactant dodecyltrimethylammonium bromide (DTMABr) and an azo dye Sunset Yellow (SSY). The lyotropic nematic phase properties of the DTMABr/1-dodecanol/water mixtures containing SSY were studied by polarizing optical microscopy, laser conoscopy, and small-angle X-ray scattering.

3. MATERIALS AND METHODS

3.1 Materials

Dodecyltrimethylammonium bromide was from Sigma. SSY was also from Sigma with a dye content of 90% and it was purified three times according to the procedure given in the Refs. (Horowitz et al., 2005; Park et al., 2008). The purity of SSY is very important to obtain reliable and reproducible results. In the literature, the phase transitions' temperatures from the nematic phase (N) to nematic+isotropic (N+I) phase coexistence ($T_{N \to N+I}$) and from N+I to the isotropic phase ($T_{N+I \to I}$) for the lyotropic chromonic mixture of 30% well-purified SSY in water were reported to be around $T_{N \to N+I}$ = 35ºC and $T_{N+I \to I}$ = 47ºC in Ref. (Edwards et al., 2008) and $T_{N \to N+I}$ = 38 ºC and $T_{N+I \to I}$ = 49 ºC, respectively, in Ref. (Joshi et al., 2009). For the same concentrations, we had $T_{N \to N+I}$ = 34.4ºC and $T_{N+I \to I}$ = 46.4ºC, with a heating rate of 0.4ºC/min by polarizing optical microscopy connected with a temperature control unit (Linkam). Thus, it was accepted that the SSY was well purified. 1-dodecanol (DDeOH) and inorganic salts were from Sigma, Merck, Aldrich and Carlo Erba in high purities (>99%). Ultrapure water was used for the preparation of lyotropic liquid crystalline mixtures (Millipore Direct-Q3 UV purification system, which produces water having 18.2 MΩ.cm of resistivity at 25ºC).

3.2 Sample Preparation

Lyotropic liquid crystalline mixtures with and without SSY were prepared into well-sealed glass test tubes, and then well-homogenized by occasionally applying vortex and centrifuging at 25°C using a temperature-controlled centrifuge. No extra heat was applied to the samples during the preparation step. A small amount of water-based ferrofluid (Ferrotec) was added into the samples at a concentration of 1 μL per 1 g of the mixture. In this way, it was possible to obtain well-oriented nematic samples under the magnetic field for polarizing optical microscopy, laser conoscopy, and small-angle X-ray scattering.

The mixtures were prepared in three different series in order to investigate the effects of (a) the co-surfactant 1-dodecanol and electrolyte NaBr, Table 3.1, (b) the Hofmeister anions, Table 3.2, and (c) the concentration of SSY, Table 3.3, on the stabilization of the lyotropic nematic phases.

Table 3.1. Compositions of the lyotropic mixtures by changing the concentrations of 1-dodecanol and NaBr. X:mole fraction percent.

Mixture	X_{DTMABr}	X_{NaBr}	X_{DDeOH}	X_{water}
s1	4.970	0.318	1.778	92.924
s2	4.969	0.316	1.821	92.894
s3	4.968	0.315	1.852	92.865
s4	4.974	0.263	1.789	92.974

Table 3.2. Compositions of mixtures containing different types of Hofmeister anion. Mixture identification, electrolyte used in the mixtures, substance concentrations in the mixture given in molar fraction percent (X).

Mixture	Electrolyte	X_{DTMABr}	$X_{electrolyte}$	X_{DDeOH}	X_{water}
s5	$NaNO_3$	4.974	0.263	1.789	92.974
s6	$NaClO_3$	4.974	0.263	1.789	92.974
s7	NaI	4.974	0.263	1.789	92.974
s8	Na_2SSY*	4.974	0.263	1.789	92.974
s9	NaSCN	4.974	0.263	1.789	92.974
s10	$NaClO_4$	4.974	0.263	1.789	92.974

* Since the SSY molecule contains two $–SO_3^-$ anionic groups, its number of moles is taken as ½ times relative to other Na salts (electrolytes) in the lyotropic mixtures. In other words,since SSY consists of two Na^+ ions and its anionic part (SSY^{2-}) has two $–SO_3^-$ anionic groups with the total charge 2−, its mole number was multiplied by the factor 2 in the calculations. In this way, the number of ions to adhere to the micelle surfaces was kept constant in all mixtures.

Table 3.3. Compositions and molar percentage (X) of substances in mixtures containing different concentrations of SSY.

Mixture	X_{DTMABr}	X_{SSY}	X_{DDeOH}	X_{water}
s11	4.988	0.000	1.794	93.218
s12	4.985	0.053	1.793	93.169
s13	4.982	0.106	1.792	93.120
s14	4.980	0.132	1.792	93.096
s15	4.980	0.158	1.791	93.071
s16	4.978	0.185	1.791	93.046
s17	4.977	0.212	1.790	93.021
s18	4.975	0.238	1.790	92.997
s19	4.973	0.289	1.789	92.949
s20	4.970	0.318	1.788	92.924
s21	4.970	0.342	1.788	92.900
s22	4.969	0.368	1.787	92.875
s23	4.966	0.421	1.786	92.826
s24	4.963	0.474	1.785	92.778

3.3 Texture Analysis by Polarizing Optical Microscopy

The textures were analyzed in a polarizing optical microscope (Nikon Eclipse E200POL, Japan). A small amount of the lyotropic sample was transferred into 0.2 mm of flat capillaries (Vitrocom, Japan). Because the lyotropic mixtures are very sensitive to the concentration change, both ends of the microslides were closed with a specific photopolymer (Medental A1, USA), on which UV-light was applied, to prevent water loss. Then, the capillaries were put in a precise temperature-control unit (Linkam LTS120E with temperature stability of, at least, 0.1ºC) with water circulation (Polyscience SD07R with an accuracy of ±0.04ºC) to provide a homogenous heat distribution in the temperature control unit.

3.4 Laser Conoscopy

Laser conoscopy is a very useful technique to determine the temperature dependence of the birefringences of the nematic phases with accuracy better than 10^{-4}. For the measurements, 2.5 mm thick lyotropic samples were prepared by putting them into a sample holder made of two discs of optical glasses separated by a 2.5 mm thick glass ring (Hellma). The temperature was controlled by a Lakeshore 335 model temperature controller (with Pt102 sensor and accuracy of ±0.001ºC) and the heat distribution to all systems was provided by a water circulating bath (Polyscience AD07R) with a precision of ±0.01ºC. The laboratory frame axes were chosen as follows: while two orthogonal axes 1 and 2 forms a horizontal plane consisted, axis 3 is vertical to it. The laser beam propagates along axis 3 and the magnetic field direction is parallel to the axis 1. This configuration leads to three different refractive indices, defined as n_1, n_2, and n_3. Then, two optical birefringences are evaluated: $\Delta n = n_2 - n_1$ and $\delta n = n_3 - n_2$. The experimental set-up had a HeNe laser (λ = 632,8 nm) and the static magnetic field (~2.04 kG) to align the samples was provided by a Walker Sci. electromagnet. The alignment procedure for the laser conoscopy was described elsewhere (Akpinar et al., 2012a).

3.5 Small-angle X-ray Scattering

Small-angle X-ray scattering (SAXS) measurements were taken with a Xeuss 2.0 laboratory-based system (Xenocs, France). The monochromatic and collimated incident X-ray beam has a square cross section with 0.7 mm side in sample’s position and wavelength of 1.5419 Å. The beam is generated by a Genix^{3D} beam delivery system, which consists of a Cu anode microfocus' X-ray source and a FOX^{3D} X-ray mirror, and it is further collimated by two sets of *scatterless* slits. The measurements were taken in transmission geometry at a sample-to-detector distance of 936 mm.

The images of the two-dimensional X-ray scattering patterns were measured by a Pilatus 300K detector (Dectris, Switzerland). The samples were put into cylindrical borosilicate glass capillaries of 1.5 mm diameter, known as Mark-tubes (Hilgenberg, Germany). The open end of each capillary was closed with a UV-sensitive photopolymer. For each measurement, a capillary was placed inside a temperature-controlled sample holder with precision of ± 0.2 °C. Rectangular bars of permanent NdFeB magnets were attached to the sidewalls of the sample holder to generate a sufficiently homogeneous magnetic field of about 1 kG in sample's position.

The SAXS measurements and analysis procedures follow closely those set out in (Galerne et al., 1987; Neto et al., 1985). The sample's alignment procedure in the magnetic field in order to have a well-aligned single domain of each nematic phase is the same as that for laser conoscopy (Galerne et al., 1987; Galerne and Marcerou, 1985). A local frame of reference was defined with Axis 1 parallel to the magnetic field in the horizontal direction, Axis 3 parallel to the capillary long axis along the vertical direction, and Axis 2 perpendicular to both axes. By a rotation of 90° of the sample's capillary together with the magnets around Axis 3, the X-ray beam can propagate along the directions of Axis 1 or Axis 2, i.e., parallel or perpendicular to the magnetic field directions, respectively. After sample's alignment at a given temperature and respective nematic phase (N_D, N_C or N_B), it was measured in two perpendicular orientations, due to the nematic phases symmetries (Neto et al., 1985): (i) with the X-ray beam along Axis 2 and therefore perpendicular to the magnetic field direction; and (ii) with the X-ray beam along Axis 1 and therefore parallel to the "magnetic field" direction. However, in case (ii), as the permanent magnets would block the X-ray beam, they were removed, and the measurement of an image took at most 30 minutes to avoid loss of sample's alignment. It was verified that, after alignment in magnetic field, it takes some hours to the significant loss of our samples' alignments in the absence of magnetic field. In case (i), as the magnets are always present, the measurement time of an image varied from 30 minutes to one hour. Each sample was measured in all its nematic phases at these two orientations, (i) and (ii), by changing its temperature and taking into account the laser conoscopy results.

The 2D X-ray scattering patterns for the aligned nematic phases were anisotropic. Therefore, two azimuthal averages were applied in each image, around the Axis 1 or 2 directions and around the Axis 3 direction, in an azimuthal angular range of $\Delta\chi = 20^{\circ}$. The azimuthal averaging, image's corrections for solid angle and for beam polarization, and noise and capillary scattering subtractions were applied using a homemade Python software using the fabio (Knudsen et al., 2013) and pyFAI (Ashiotis et al., 2015) libraries. Finally, for each image there result two scattering curves of scattering intensity as a function of the scattering vector modulus $q = (4\pi/\lambda)\ sin\ \theta$, where 2θ is the scattering angle. Due to the geometry of the experimental setup, there results a useful q range of $0.01 < q < 0.18$ Å^{-1} in the Axis 1 or 2 directions and of $0.01 < q < 0.37$ Å^{-1} in the Axis 3 direction.

4. RESULTS AND DISCUSSIONS

4.1 Polarizing Optical Microscopy

The textures of the different lyotropic phases were observed in a polarized optical microscope between crossed polarizers in the temperature range from 10°C to 50°C. This study is concerned only with the nematic phases; therefore, the partial phase diagrams have been investigated up to the phases or the phase coexistence regions adjacent to the nematic phase regions. At low temperatures, a white and highly turbid texture was observed, most probably from a 'coagel' phase (Figure 4.1a). An isotropic phase rich two-phase (2P) region was observed at high temperatures next to the nematic region, Figure 4.1b. The nematic phase textures obtained from all mixtures have a characteristic "Schlieren" structure and similar textures were observed in all nematic phase yielding mixtures. As an example, the textures of the s8 mixture are given in Figures 4.1 and 4.2.

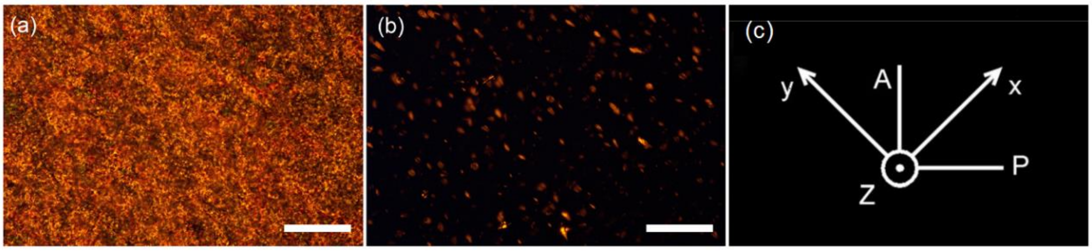

Figure 4.1. Textures of mixture s8, whose composition is given in Table 3.2: (a) a gel-type phase texture observed at 10°C, and (b) a two phases (2P) texture at 45°C. The white bar represents 200 μm. (c) x, y and z are the laboratory frame axes; P and A are the directions of polarizer and analyzer, respectively. The long capillary axis is parallel to the y-axis. Same geometry of the experiment was applied to the textures given in Figure 4.2.

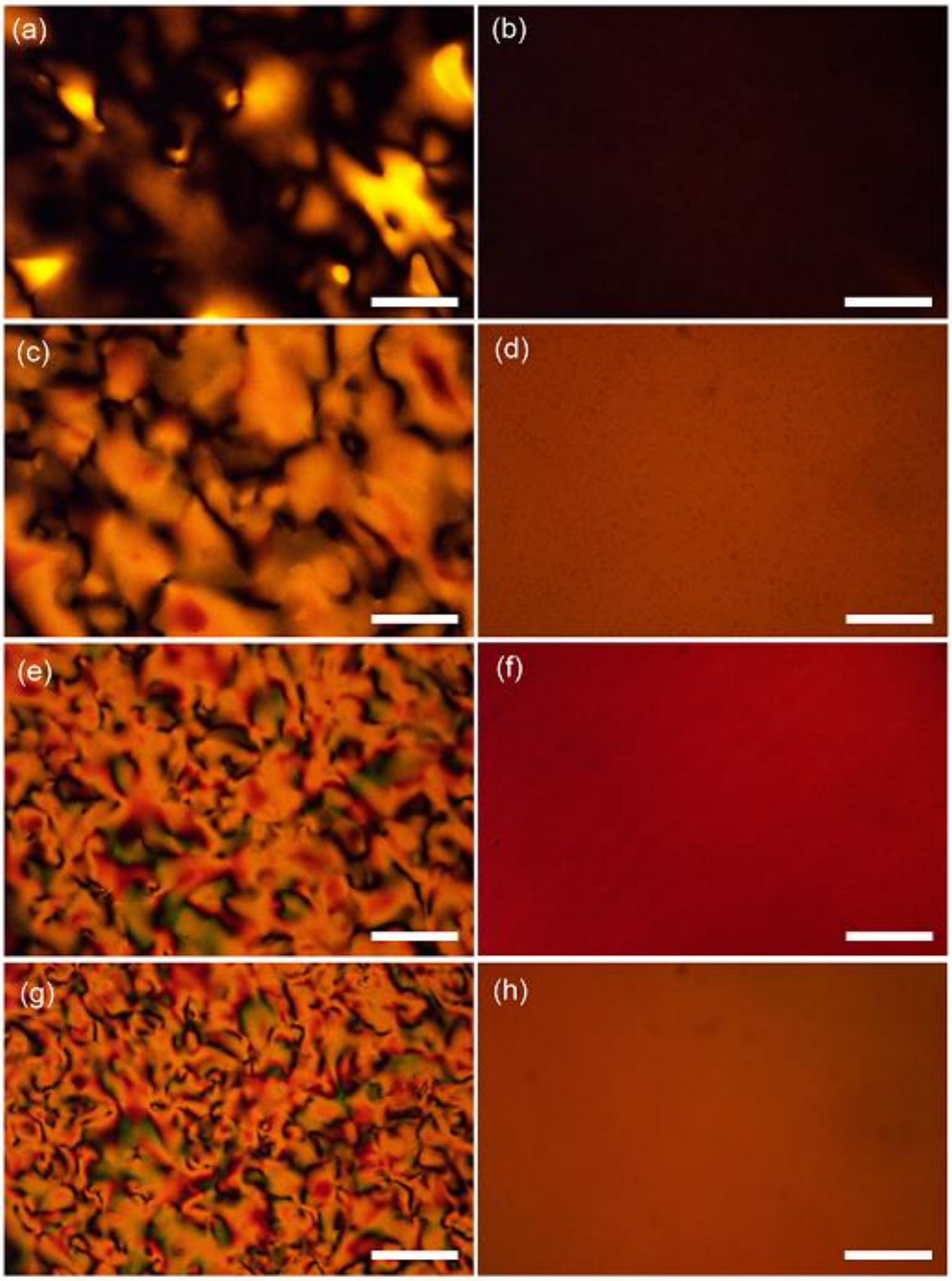

Figure 4.2. Textures of non-aligned nematic phases in the absence of magnetic field for the mixture s8 from: (a) N_D phase at 23°C; (c) N_B phase around the N_D-N_B phase transition at 21°C; (e) N_B phase around the N_B-N_C phase transition at 17.2°C; (g) N_C phase at 15°C. Well-aligned textures of those nematic phases by applying a magnetic field of 0.9 kG along x-axis direction, as shown in Figure 4.1c: (b) 23°C; (d) 21°C; (f) 17.2°C; (h) 15°C. The white bar represents 200 μm.

4.2 Analysis of Small-angle X-ray Scattering Measurements

Tables 4.1 and 4.2 show the results for the average dimensions (A, B, C) of the available volume per micelle for all the samples measured by SAXS. The values of (A, B, C) for each sample were measured from the 2D SAXS patterns according to Galerne et al (Boden et al., 1987).

Table 4.1. Average dimensions (A, B, C) of the available volume per micelle for some samples of Table 3.2. These results were also used for the parameters' calculations of Table 4.5.

Mixture	**A (Å)**	**B (Å)**	**C (Å)**
s7	60.8 ± 1.9	49.4 ± 0.7	44.0 ± 0.2
s8	61.3 ± 1.2	49.6 ± 0.6	43.8 ± 0.1
s9	62.6 ± 1.3	50.2 ± 0.8	43.7 ± 0.2
s10	65.8 ± 2.0	51.0 ± 0.9	43.6 ± 0.1

Table 4.2. Average dimensions (A, B, C) of the available volume per micelle for some samples of Table 3.2 and Table 3.3. These results were also used for the parameters' calculations of Table 4.7.

Mixture	**A (Å)**	**B (Å)**	**C (Å)**
s8	61.3 ± 1.2	49.6 ± 0.6	43.8 ± 0.1
s19	62.2 ± 1.4	50.2 ± 1.0	43.7 ± 0.1
s20	63.3 ± 1.1	51.7 ± 0.7	43.6 ± 0.1
s23	66.7 ± 1.4	54.9 ± 0.7	43.3 ± 0.2

For the analysis of the SAXS results, intrinsic biaxial micelle, or IBM, model was assumed (see the part 1.1.1.2 for more information) (Galerne et al., 1987; Neto et al., 1985). Remember that, in this model, the micelles are supposed to have approximately the same average shape with an orthorhombic or biaxial symmetry in the three nematic phases. Therefore, as a first order approximation, both the available volume per micelle and the micelle itself have the average shape of a rectangular parallelepiped, as sketched in Figure 4.3. The typical dimensions of the available volume per micelle are A, B, C and were measured by SAXS as presented in the previous section. This model was used here for an estimate of the average micelle's aggregation number (N_{agg}), of the average polar layer thickness (w_{polar}), of the micelle's core average dimensions (A′, B′, C′), and of the average area per polar head (a_0).

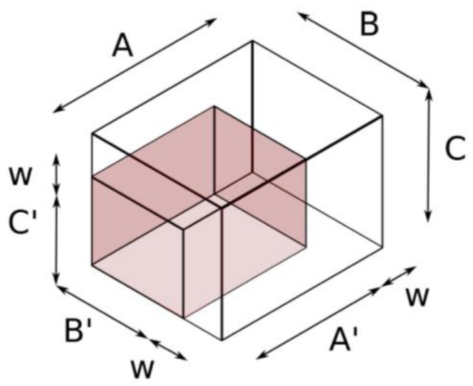

Figure 4.3. Schematic representation of the average available volume per micelle with dimensions A, B, C, and of the micelle's hydrocarbon core with dimensions A′, B′, C′, represented by the colored part. The polar layer around the micelles' core is supposed to be of uniform thickness w.

The total available volume is divided in two parts. The first part is the hydrophobic core composed of the hydrocarbon chains of the surfactant and the cosurfactant. It is represented by the colored part in the sketch of Figure 4.3 and has dimensions A′, B′, C′, where C′ is the main surfactant bilayer dimension by definition. Henceforward, the quantities related to the micelle's core will be indexed by the word *core*. The second part is the layer around the micelle's hydrophobic core. This layer is composed of the surfactants' polar groups attached to the hydrophobic core surface, and a water layer that occupies the rest of the volume with dissociated ions of the electrolytes and counter ions from the main surfactant.

Henceforward, this layer will be called polar layer and the related quantitites will be indexed by the word *polar*.

For a unit of the available volume per micelle, the relation between its total mass m and its volume V is given by

$$m = \bar{\rho}V \tag{4.1}$$

where $\bar{\rho}$ is the average density over all the volume. As the samples present homogeneous nematic phases, this average microscopic density is assumed to be equal to the macroscopic density of the sample and it is supposed here $\bar{\rho}\sim 1.0$ g/cm^3 for all of the samples.

Similarly, the mass and volume of the micelle's hydrophobic core are related by

$$m_{core} = \bar{\rho}_{core}V_{core} \tag{4.2}$$

where $\bar{\rho}_{core}$ is its average density. The hydrophobic core is composed of the single saturated hydrocarbon chains of the surfactant and cosurfactant. As discussed by Tanford (Tanford, 1980), the hydrocarbon chains in the core are in a liquid-like state, so that $\bar{\rho}_{core}$ can be approximated by the typical density of liquid hydrocarbons, i.e., $\bar{\rho}_{core}$ = 0.8 g/cm^3.

From the above relations,

$$\frac{V_{core}}{V} = \left(\frac{\bar{\rho}}{\bar{\rho}_{core}}\right)\phi_{core} \tag{4.3}$$

where $\phi_{core} = \frac{m_{core}}{m}$ is the micelle's core mass fraction. By the reasoning used for $\bar{\rho}$ above, ϕ_{core} is supposed to be equal to the macroscopic mass fraction of the hydrocarbon chains in relation to the total mass of the sample. Observe that no hipothesis for the shapes of the parts were necessary for the above calculations.

The total mass of each substance in each sample is known from the preparation procedure. Thus, the core's mass fraction for each sample was estimated by the ratio between the total mass of surfactants' hydrocarbon chains and the total mass of the sample. Both surfactant and cosurfactant were considered. The main surfactant DTMABr molecule $C_{15}H_{34}NBr$, with M_{DTMABr} = 308.34 g/mol, was divided in two parts, the polar head $–(CH_2)N^+(CH_3)_3$ with molar mass $M_{DTMABr}^{head} =$ 73.14 g/mol, and the hydrocarbon chain $–(CH_2)_{10}CH_3$, with $M_{DTMABr}^{chain} = 155.30$ g/mol, that composes the liquid hydrocarbon core. Similarly, for the cosurfactant 1-dodecanol $C_{12}H_{26}O$, with M_{DDeOH} = 186.33 g/mol, the polar head is $–(CH_2)OH$ with $M_{DDeOH}^{head} =$ 31.03 g/mol, and the hydrocarbon chain is $–(CH_2)_{10}CH_3$, with $M_{DDeOH}^{chain} =$ 155.30 g/mol. Thus, $M_{DTMABr}^{chain}/M_{DTMABr}$ of the total mass of DTMABr plus $M_{DDeOH}^{chain}/M_{DDeOH}$ of the total mass of 1-dodecanol are the total mass of hydrocarbon chains in a sample that form the micelles' core.

The hydrophobic portions of both surfactants are single saturated hydrocarbon chains. The volume v of a chain is given by Tanford's empirical formula (Tanford, 1980) , in Å^3,

$$v = 27.4 + 26.9n_c' \tag{4.4}$$

where n_c' is the number of carbon atoms per chain that are embedded in the micelle core, and, as in the previous paragraph, n_c' = 11 for both molecules. Therefore, the average aggregation number N_{agg} of a micelle is given by

$$N_{agg} = \frac{V_{core}}{v} = \phi_{core}\left(\frac{\bar{\rho}}{\bar{\rho}_{core}}\right)\frac{V}{v} \tag{4.5}$$

In order to calculate N_{agg}, now it is assumed a shape for the average available micellar volume, that of a rectangular parallelepiped, and, therefore, V = ABC.

To calculate other structural parameters, additional hypotheses are necessary. But first some parameters are defined. The surface area of the available micellar volume is S = 2 (AB + AC + BC), and the sum of the sides or "perimeter" of the average available micellar volume is P = A + B + C. By the model of Figure 4.3, the average available micellar volume is given by

$$V = V_{core} + V_{polar} \tag{4.6}$$

and, therefore, using equation 4.3,

$$V_{polar} = V - V_{core} = V\left[1 - \left(\phi_{core}\frac{\bar{\rho}}{\bar{\rho}_{core}}\right)\right] \tag{4.7}$$

All the quantities of the last term are known.

V_{polar} can also be calculated by the geometrical model of Figure 4.3 with the additional hypotheses of uniform thickness w_{polar} of the polar layer around the micelle's hydrocarbon core, and of the shape of this hydrophobic core. It implies that,

$$\left.\begin{aligned} A &= A' + w_{polar} \\ B &= B' + w_{polar} \\ C &= C' + w_{polar} \end{aligned}\right\} \tag{4.8}$$

and that,

$$\begin{aligned} V_{polar} &= V - V_{core} \\ &= ABC - A'B'C' \\ &= ABC - (A - w)(B - w)(C - w) \\ &= ABC - ABC + ABw + ACw - Aw^2 + BCw - Bw^2 - Cw^2 + w^3 \\ &= (AB + AC + BC)w - (A + B + C)w^2 + w^3 \\ &= \frac{S}{2}w - Pw^2 + w^3 \end{aligned}$$

where the definitions of S and P given above were used in the last line, and the subscript polar were omitted from w for economy. Therefore,

$$w_{polar}^3 - Pw_{polar}^2 + \frac{S}{2}w_{polar} - V_{polar} = 0 \tag{4.9a}$$

or

$$w_{polar}^3 - Pw_{polar}^2 + \frac{S}{2}w_{polar} - V\left[1 - \left(\phi_{core}\frac{\bar{\rho}}{\bar{\rho}_{core}}\right)\right] = 0 \tag{4.9b}$$

where equation 4.7 was used for the coefficient V_{polar}. Thus, there results a cubic equation for the indeterminate w_{polar}.

All the coefficients can be calculated from the results of measurements or estimated for each sample. The coefficients P, S and V were calculated for each sample from the results for A, B, C of Tables 4.1 and 4.2. $\bar{\rho}$ and $\bar{\rho}_{core}$ were estimated above and assumed the same for all samples. Thus, for each sample, there is a cubic equation in w_{polar} with coefficients from experimental quantitites with uncertainties.

Once w_{polar} is known by solving the cubic equation for a given set of coefficients and their respective uncertainties, the average dimensions A′, B′, C′ of the micelles core can be calculated from equation 4.8. Also, the average area per polar head group, a_0, in the micelle's core surface is given by,

$$a_0 = \frac{2(A'B' + A'C' + B'C')}{N_{agg}} \tag{4.10}$$

The usual propagation of uncertainties was used to estimate the uncertainties in all quantitites calculated above.

The cubic equation for the polar layer thickness w_{polar} can be solved for each sample with the set of average parameters A, B, C given in Tables 4.1 and 4.2. Figure 4.4 shows an example of a graphical method to solve this equation. First, it is rewritten in the form (equation 4.9b),

$$w_{polar}^3 - Pw_{polar}^2 + \frac{S}{2}w_{polar} - V\left[1 - \left(\phi_{core}\frac{\bar{\rho}}{\bar{\rho}_{core}}\right)\right]$$

Then, in Figure 4.4, the expression on the left is represented by the blue curve named "V_{polar} from the proposed geometry", and the right term by the constant black curve named "V_{polar} from the densities". The intersection of these curves gives the solution of the equation for w_{polar}.

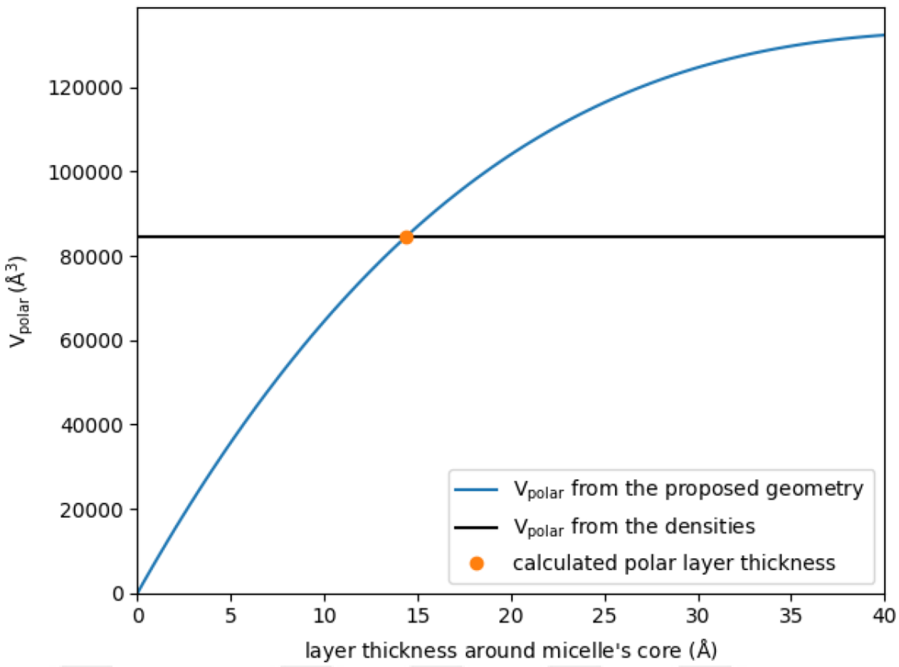

Figure 4.4. Graphical method to solve the cubic equation 4.9b given a set of average parameters A, B, C. In this example, the parameters for sample s8 of Table 4.2 were used.

This graphical procedure could be repeated for the cubic equation of all the samples, for the calculation of their average polar layer thickness w_{polar}. However, the coefficients of the polynomials are calculated from experimental quantitites and, therefore, they are not exact quantitites, i.e. they have uncertainties estimated by the usual propagation method.

Thus, a Monte Carlo-type method was used to solve these cubic equations with coefficients with uncertainties. First, it was supposed that the coefficients P, S and V_{polar} of equation 4.9b obey a normal distribution with mean values given by the values of the coefficients P, S or V_{polar} calculated from the average values of A, B, C, and standard deviations given by the usual propagation formulas. Then, a given set of these three coefficients were drawn from these normal distributions using a pseudo-random number generator. Finally, the drawn cubic equation were solved completely by a numerical root-finding algorithm and the real solution in the range (0, C′) were taken as a possible value for w_{polar}.

This procedure was repeated 50000 times for each sample, i.e. for each set of values A, B, C given in Tables 4.1 or 4.2, 50000 polynomials were solved for w_{polar}.

So that, a distribution of real solutions w_{polar} results for each sample, of which a mean and a standard deviation values for w_{polar} could be calculated.

An example is given for sample s8 from Table 4.2. Figure 4.5 shows the final distributions of drawn coefficients P, S and V_{polar} from the normal distribution in red. Figure 4.6 shows the distribuition of all the roots of the drawn from 50000 cubic polynomials in the complex plane. The colormap measures the absolute frequency of solutions in a given region of the complex plane. Observe the set of solutions over the real axis.

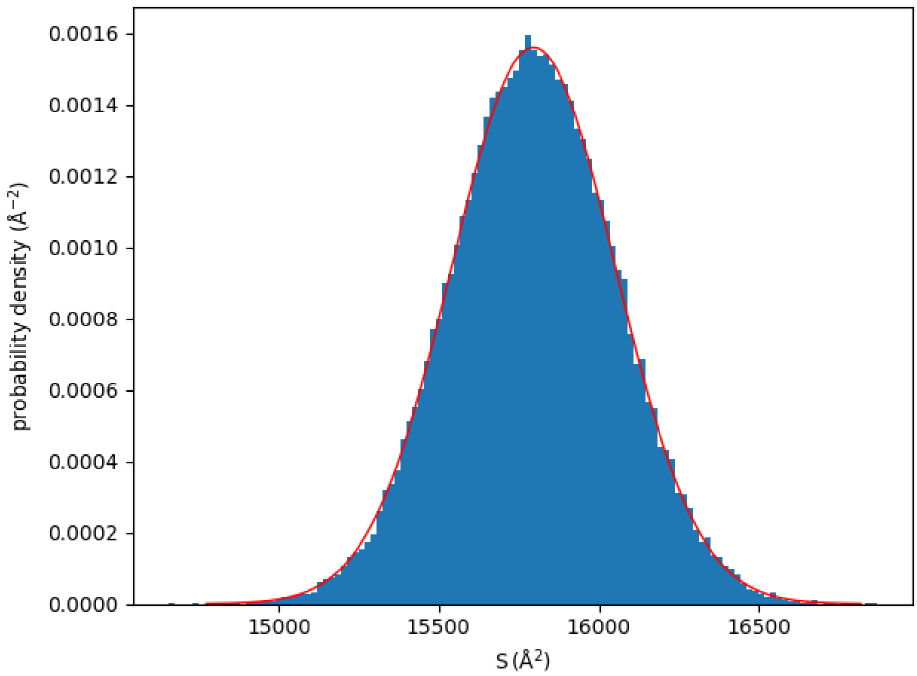

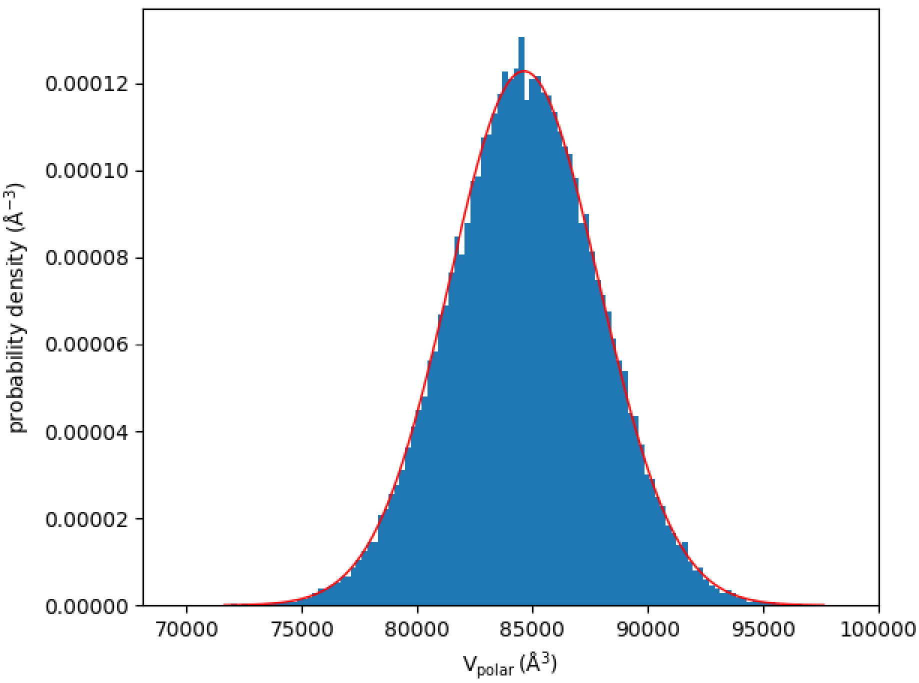

Figure 4.5. Distributions of the polynomials' coefficients P, S and V_{polar} of equation 4.9b for sample s8. The coefficients were generated by a pseudo-random number generator from a normal distribution, drawn in red, with mean values given by the values of these *P*, *S* or V_{polar} calculated from the average values of A, B, C, and standard deviations given by the usual propagation formulas. 50000 samples were drawn for each distribution.

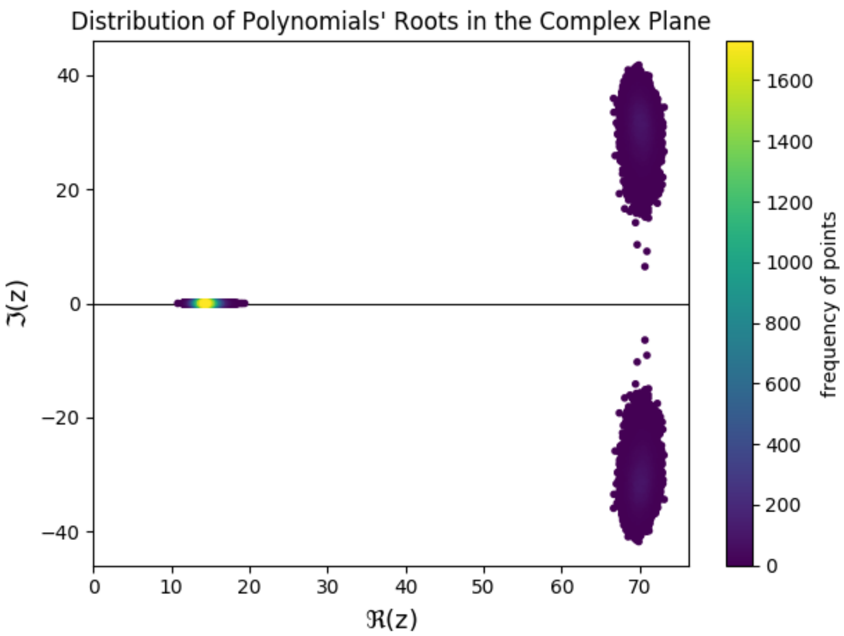

Figure 4.6. Distribution of all the roots of the cubic polynomials of sample s8 in the complex plane. The colormap measures the absolute frequency of solutions in a given region of the complex plane. 50000 cubic equations were solved for each sample.

The complex solutions were discarded and only the real solutions in the range (0, C′) were taken into account. Figure 4.7 shows the distribution of the real roots of the cubic polynomials. These are the roots over the real axis in Figure 4.6. The mean and standard deviation of this distribution were taken as the average polar layer thickness w_{polar} and its uncertainty, respectively. Observe that no probability density model was fitted to this distribution.

The values of the average polar layer thickness w_{polar} and its uncertainty calculated this way were used for the calculations of the parameters in the end of the previous section. The results for w_{polar} and those parameters are shown in Tables 4.5 and 4.7.

All the mentioned numerical calculations, pseudo-random number generator, root-finding routines, and figures were made using the Python programming language and its numerical (NumPy), scientific (SciPy) and visualization (Matplotlib) libraries.

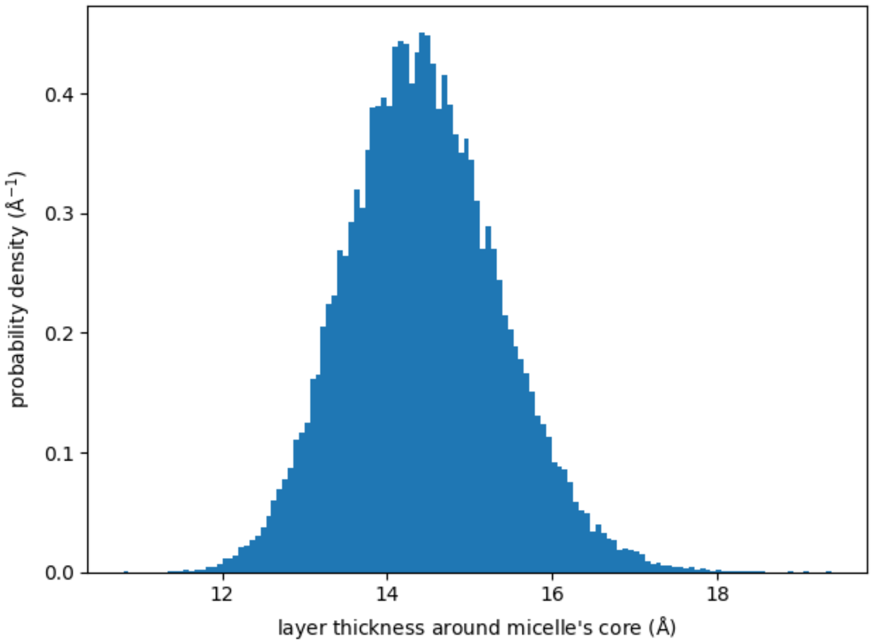

Figure 4.7. Distribution of the real roots w_{polar} of the cubic polynomials of sample s8. These are the roots over the real axis in Figure 4.6. 50000 cubic equations were solved for each sample.

4.3 Effects of Cosurfactant and Electrolyte on the Properties of Lyotropic Nematic Phases

Before understanding the effect of the dye-surfactant interactions on the properties of the DTMABr/Sunset Yellow lyotropic mixtures, the roles of the cosurfactant and the electrolyte used in the preparation of the lyotropic liquid crystal mixtures need to be well understood. Long-chain alcohols, such as 1-decanol, are generally used as cosurfactants to form lyotropic liquid crystal mixtures (Yu and Saupe, 1980). The surfactant molecule dodecyltrimethylammonium bromide, as we brought to the literature previously, may give lyotropic liquid crystal mixtures with 1-dodecanol (Akpinar et al., 2014; Akpinar et al., 2015). One of the mixtures given in previous studies (Akpinar et al., 2014; Akpinar et al., 2015) was selected as the starting point (Table 4.3, mixture s3) and three lyotropic mixtures were prepared by adding 1-dodecanol in three different concentrations (s1, s2 and s3). As can be seen from the laser conoscopy results in Figure 4.8 and from Table 4.3, with the increasing amount of 1-dodecanol in the mixture, both N_D-N_B and N_B-N_C phase transitions shift to lower temperatures, while N_D and N_B phases temperature ranges increase, and N_C phase region decreases. Furthermore, around both N_D-N_B (maximum value in N_D phase region) and N_B-N_C (minimum value in N_C phase region) transitions, the birefringence values increased with the increasing amount of 1-dodecanol. This corresponds to an increase in micelle size or micellar shape anisotropy (Neto and Salinas, 2005; Akpinar et al., 2019b). Thus, the 1-dodecanol molecule causes N_D phase stabilization and also causes the growth of micelles.

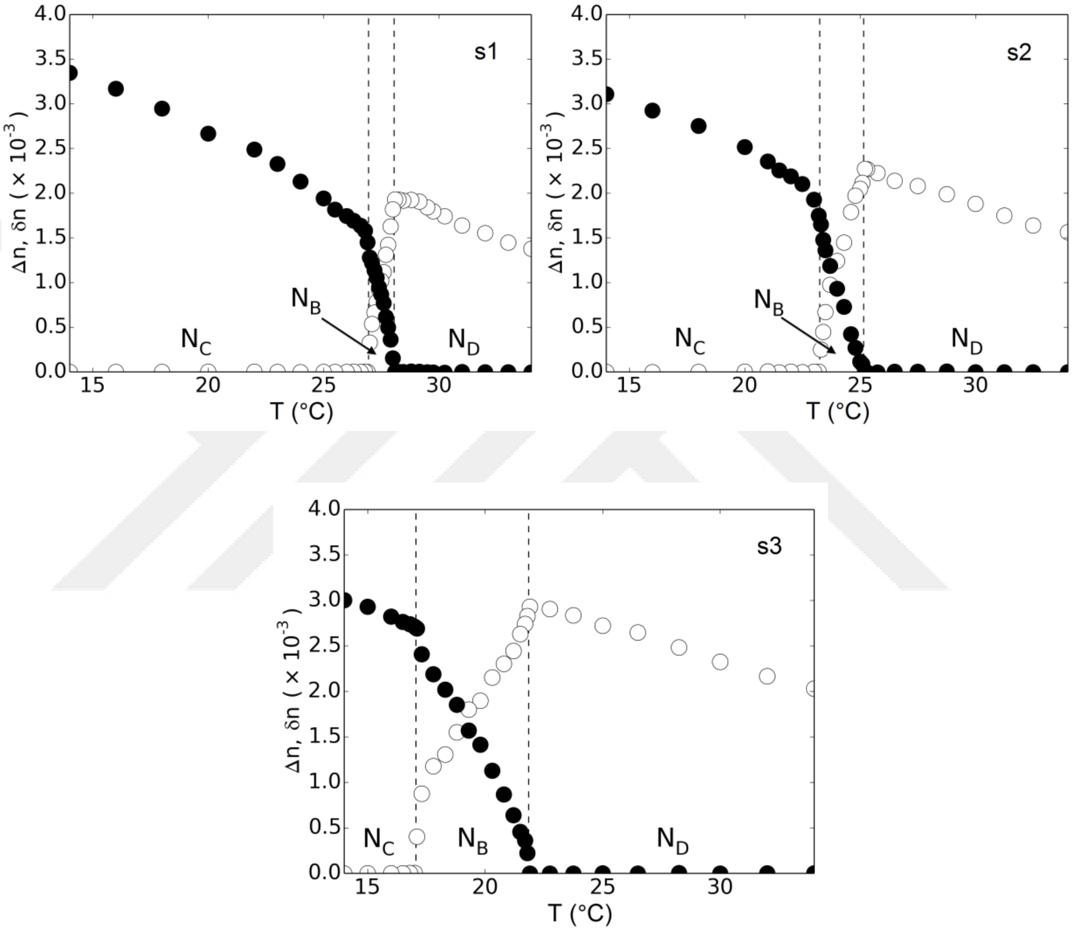

Figure 4.8. Birefringences as a function of temperature for the mixtures given in Table 1. Δn (●) and δn (○).

Table 4.3. Phase transition temperatures of the lyotropic mixtures by changing the concentrations of 1-dodecanol (s1-s3) and NaBr (s1-s4). ΔT_{N_B}: temperature range of the biaxial phase.

Mixture	Phase transition temperatures	ΔT_{N_B}/℃
s1	$N_D \xrightarrow{28.05℃} N_B \xrightarrow{26.95℃} N_C$	1.10
s2	$N_D \xrightarrow{25.15℃} N_B \xrightarrow{23.25℃} N_C$	1.90
s3	$N_D \xrightarrow{21.85℃} N_B \xrightarrow{17.05℃} N_C$	4.80
s4	$N_D \xrightarrow{30.05℃} N_B \xrightarrow{29.15℃} N_C$	0.90

Another mixture (s4) was prepared by reducing the amount of NaBr with respect to the s1 mixture. The laser conoscopy results for the s4 mixture are given in Figure 4.10-4.13. In this way, we can discuss which Hofmeister series electrolyte anion is characteristic of the anionic portion of the sunset yellow dye molecule. The results of the mixtures s1 and s4 indicate that the effect of NaBr is similar to that of 1-dodecanol, that is, (a) N_D-N_B and N_B-N_C phase transition temperatures decrease with the increasing amount of NaBr, (b) the N_D phase region increases in the partial phase diagram, and (c) the range of the biaxial phase region is increased. The most significant difference between 1-dodecanol and NaBr is that, while the amount of 1-dodecanol is increased by 4.2%, the biaxial phase range increases by 4.4 times, and while the amount of NaBr increases by 20.1%, the biaxial phase range increases only 1.2 times. Therefore, it is seen that the effect of 1-dodecanol is higher than NaBr on the biaxial nematic phase-range stabilization when the "unit amounts" in the same starting mixture are compared.

It is important to determine the properties of the azo dye molecule before proceeding to the study of the properties of mixtures containing sunset yellow (SSY). The SSY molecule is a 1:2 type electrolyte, such as Na_2SO_3 electrolyte, which includes two Na^+ ions attached to two SO_3^- groups of the anionic moieties. Therefore, when it ionizes in water, it gives one SSY^{2-} anion and two Na^+ cations to the environment. Studies have shown that SSY molecule is present in hydrazone form rather than azo form in an aqueous medium (Figure 4.9) (Edwards et al., 1996).

The hydrogen bond formed in the hydrazone form allows the molecule to have a stable planar structure (Lydon, 2010).

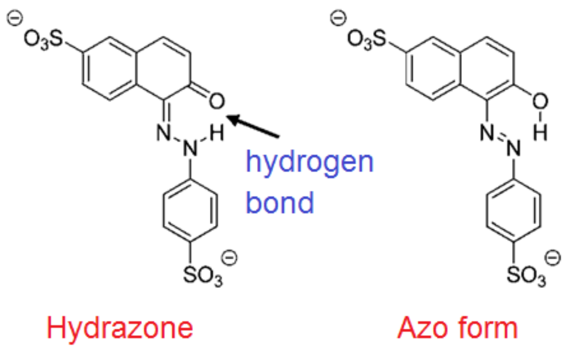

Figure 4.9. The tautomeric forms of the Sunset yellow molecule (Lydon, 2010).

The electrolytes interact with surfactant head groups on the micelle surfaces in liquid crystal mixtures, reducing repulsions between the surfactant head groups and making micellization more preferable (Kumar et al., 2012). Depending on the strength of the interactions between the electrolyte and the head groups, this shielding may be more or less effective. It has been demonstrated that those interactions are important in stabilizing different types of nematic phases (Akpinar et al., 2016a; Akpinar et al., 2016b). At this point, it is to be noted that the degrees of kosmotropic, which prefers to be more hydrated by water molecules, and chaotropic, which prefers to be less hydrated by water molecules, properties of surfactant and electrolyte ions have an important role in obtaining different types of the nematic phases. For example, the strong similarity of the surfactant head group and the electrolyte ion (kosmotropic-kosmotropic or chaotropic-chaotropic) leads to the stabilization of the lyotropic N_D phase, and the weak similarity leads to that of the lyotropic N_C phase. The lyotropic N_B phase is usually obtained in the case of moderate kosmotropic-chaotropic interactions at the micelle surfaces (Akpinar et al., 2016a). DTMABr surfactant molecule includes positively charged chaotropic ionic head group, $–N(CH_3)_3^+$, (Marcus, 2009). Therefore, negatively charged chaotropic electrolyte anions are preferably bound to this head group. Some electrolytes containing Hofmeister series anions were added to the mixtures containing DTMABr in a constant molar number, i.e. in the fixed mixture composition, as given in Tables 3.1 for s4 and 3.2 for s5-s10. Given the chaotropic properties of the selected

Hofmeister series ions, the following sequence applies (Leontidis, 2002; Wen et al., 2014):

$$Br^- < NO_3^- < ClO_3^- < I^- < SCN^- < ClO_4^-$$

In some studies, Br^- and NO_3^- sequence is also given as $Br^- \sim NO_3^-$ or $Br^- > NO_3^-$ (Umapathi et al., 2018) and this may be attributed to that the chaotropic degrees of both ions are close to each other. At this point, it is very important to determine the property of SSY^{2-} anion of the SSY molecule.

Table 4.4. Phase transition temperatures of the lyotropic mixtures containing different types of Hofmeister anion, electrolyte used in the mixtures, and temperature range of the biaxial nematic phase. ΔT_{N_B}: temperature range of the biaxial phase.

Mixture	Electrolyte	Phase transition temperatures	ΔT_{N_B}/℃
s4	NaBr	$N_D \xrightarrow{30.05℃} N_B \xrightarrow{29.15℃} N_C$	0.90
s5	$NaNO_3$	$N_D \xrightarrow{29.15℃} N_B \xrightarrow{27.95℃} N_C$	1.20
s6	$NaClO_3$	$N_D \xrightarrow{24.35℃} N_B \xrightarrow{22.35℃} N_C$	2.00
s7	NaI	$N_D \xrightarrow{24.05℃} N_B \xrightarrow{21.25℃} N_C$	2.80
s8	Na_2SSY	$N_D \xrightarrow{21.15℃} N_B \xrightarrow{17.05℃} N_C$	4.10
s9	NaSCN	$N_D \xrightarrow{19.25℃} N_B \xrightarrow{14.85℃} N_C$	4.40
s10	$NaClO_4$	N_D	-

Table 4.4 also shows nematic-nematic phase transition temperatures, and biaxial phase temperature ranges of the mixtures prepared with electrolytes containing different types of Hofmeister anions and SSY (or Na_2SSY). The nematic-nematic phase transitions were measured by laser conoscopy.

In the present study, we also calculated the invariants of the optical dielectric tensor, ϵ, as second-rank, traceless, symmetric tensor order parameter from the experimental values of the optical birefringences. In a uniaxial (biaxial) nematic phase, there are two (three) different refractive indices and the difference between the refractive indices are the optical birefringences. The birefringences Δn and δn vanish in the uniaxial N_D and N_C phases, respectively. In the N_B phase both birefringences are non-null. If the three orthogonal laboratory frame axes are chosen as 1, 2 and 3, we have three diagonal elements of the anisotropic part of the dielectric tensor (ϵ_{a1}, ϵ_{a2} and ϵ_{a3})

$$\epsilon_{a1} = -\frac{4\langle n \rangle}{3}\left(\Delta n + \frac{\delta n}{2}\right) \tag{4.11}$$

$$\epsilon_{a2} = \frac{2\langle n \rangle}{3}(\Delta n - \delta n) \tag{4.12}$$

$$\epsilon_{a3} = \frac{4\langle n \rangle}{3}\left(\frac{\Delta n}{2} + \delta n\right) \tag{4.13}$$

where $\langle n \rangle$ is the average index of refraction of the mixture. The invariants of a tensor order parameter (σ_1, σ_2 and σ_3) can be written in terms of the diagonal elements of the dielectric tensor,

$$\sigma_1 = \epsilon_{a1} + \epsilon_{a2} + \epsilon_{a3} \tag{4.14}$$

$$\sigma_2 = \frac{2}{3}(\epsilon_{a1}^2 + \epsilon_{a2}^2 + \epsilon_{a3}^2) \tag{4.15}$$

$$\sigma_3 = 4\epsilon_{a1}\epsilon_{a2}\epsilon_{a3} \tag{4.16}$$

where the first invariant σ_1 is zero (Neto and Salinas, 2005). The temperature dependences of both birefringences and the invariants, and the interdependence of invariants are given in Figure 4.10-4.13. In the following sections, the composition of the SSY molecule in mixtures will be shown as Na_2SSY.

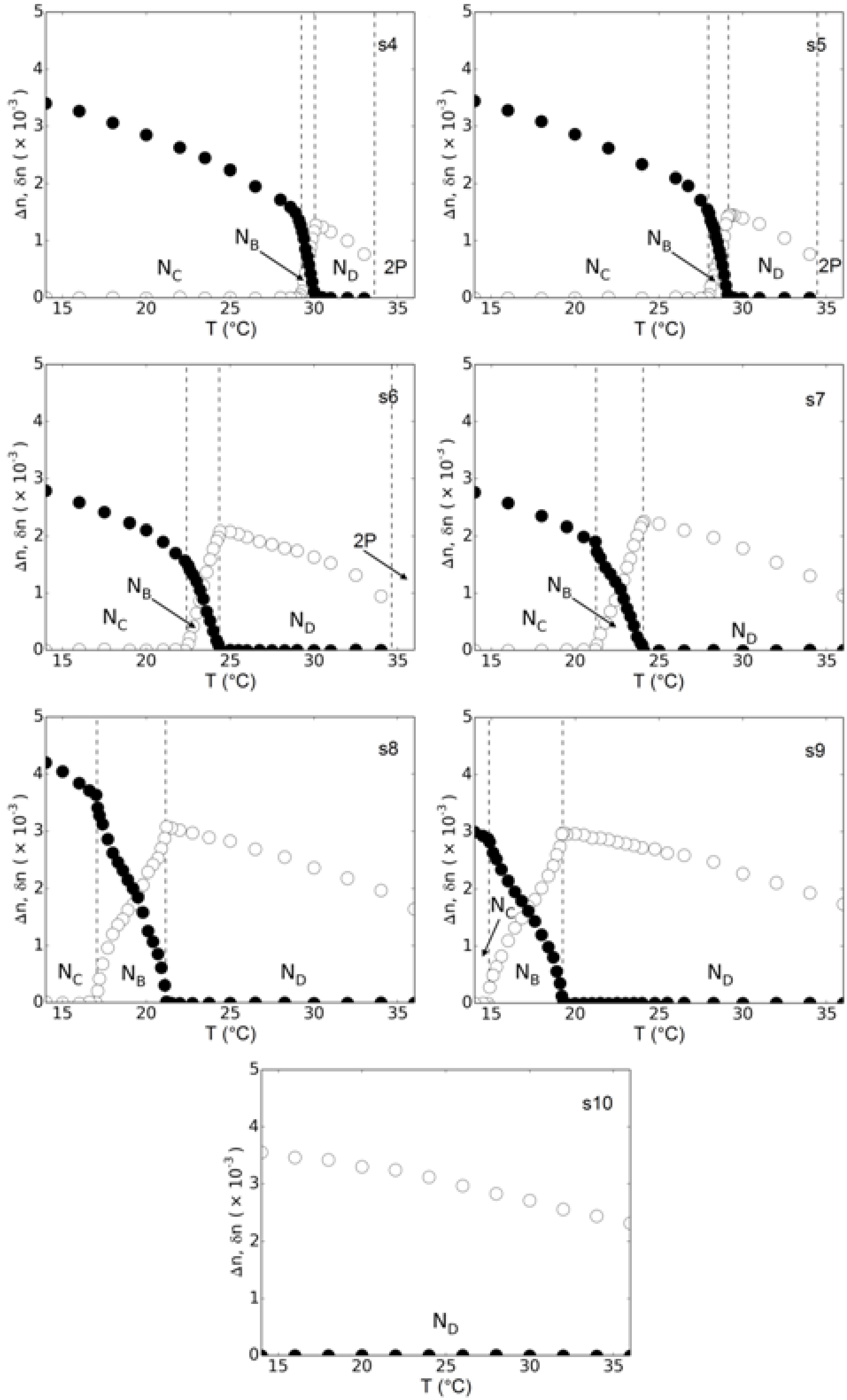

Figure 4.10. Temperature dependences of the birefringences of the mixtures given in Table 4.4. The 2P region corresponds to the two-phase region. Δn (●) and δn (○).

As can be seen from Figure 4.10, in the Hofmeister series, as the N_D and/or N_B phase temperature range increase in the partial phase diagrams, the N_C phase region decreases going from the lowest chaotropic NaBr containing mixture (s4) to the mixture with the highest chaotropic $NaClO_4$ (s10). In the mixture containing $NaClO_4$, only the N_D phase is observed. When the highest birefringence values in the N_D-N_B phase transitions, biaxial nematic phase regions, and uniaxial-biaxial phase transition temperatures are compared in the N_D phase regions, it is seen that the SSY molecule has approximately the same chaotropic behavior as NaSCN. This is also proved by SAXS results, as shown in Table 4.5. This is an important result because, when investigating the interaction of SSY molecule with the surfactant systems, it will be interesting to select the surfactant molecules according to this feature.

The temperature dependences of σ_2 and σ_3 shown in Figures 4.11 and 4.12 (Hofmeister anions) are consistent with the literature (Neto and Salinas, 2005). As can be seen from Figure 4.13, showing the interdependence of σ_2 and σ_3 values, as the chaotropic properties of anions in Hofmeister series increase, σ_2 and σ_3 values increase. The interesting point here is that both σ_2 and σ_3 values decrease in the biaxial phase region in the mixtures of all Hofmeister anions (except the mixture s10), while σ_2 values for the mixture of the SSY molecule (mixture s8) increase.

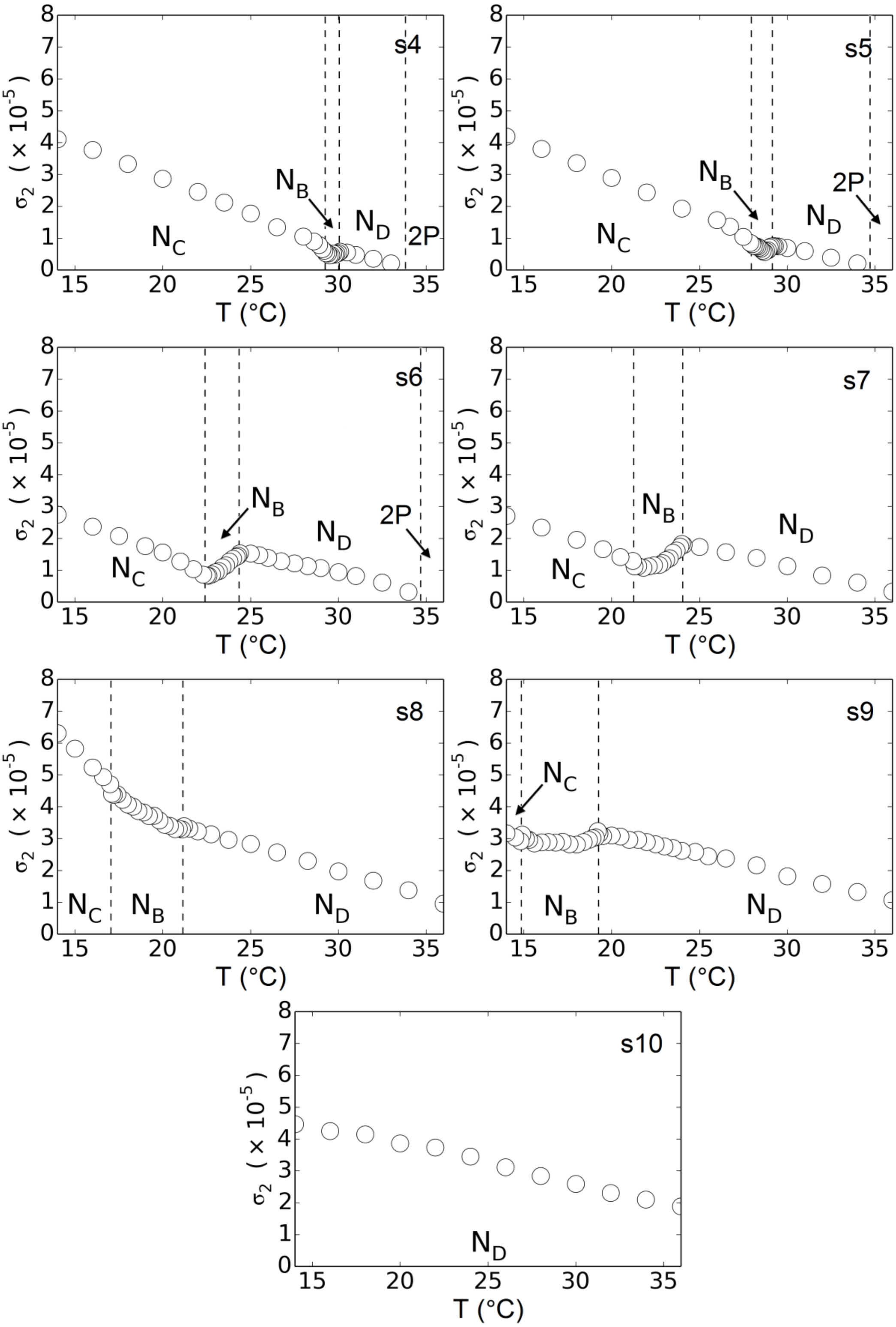

Figure 4.11. Temperature dependence of the invariant σ_2 obtained from laser conoscopy for the mixtures given in Table 4.4. The 2P region corresponds to the two-phase region

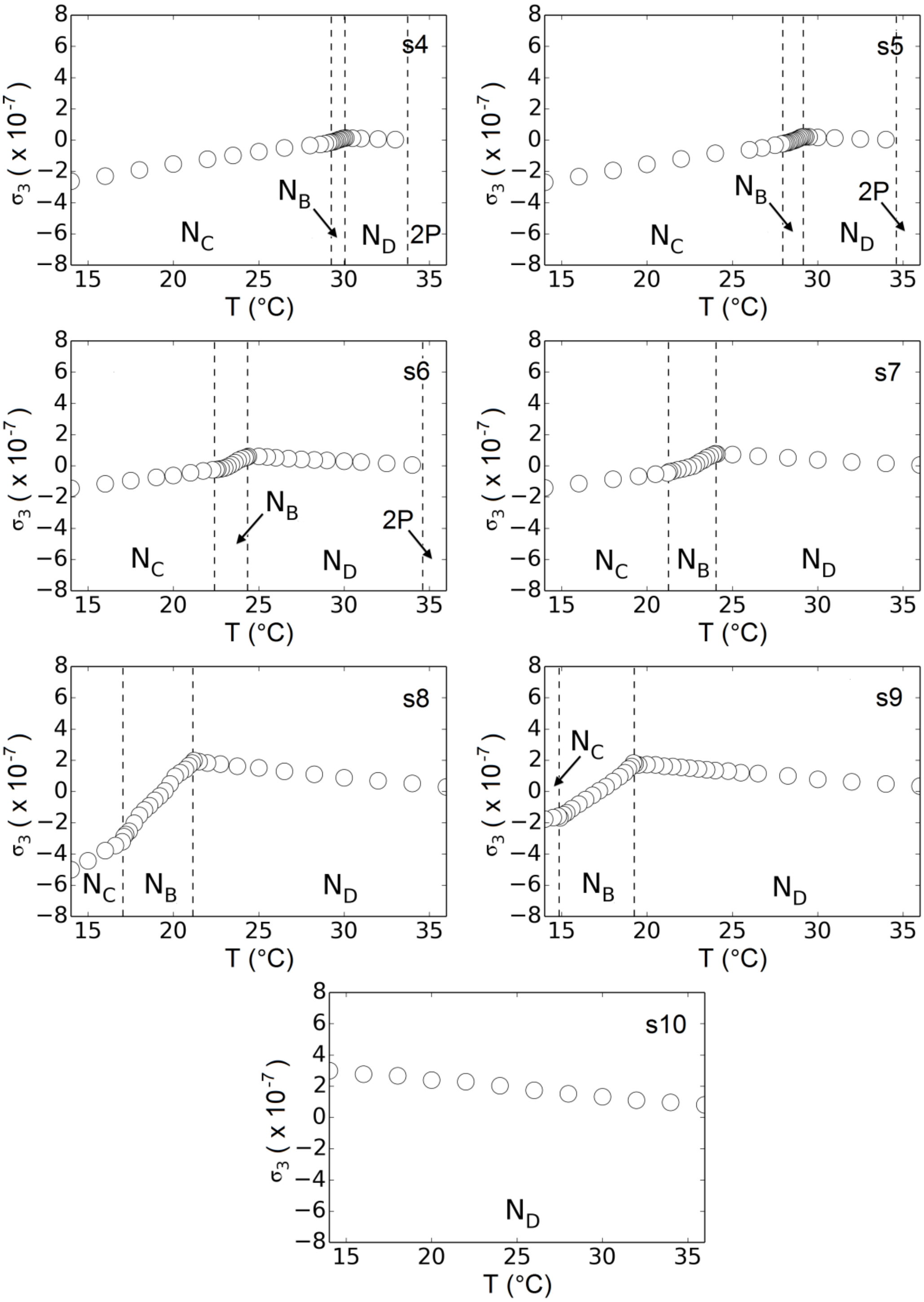

Figure 4.12. Temperature dependence of the invariant σ_3 obtained from laser conoscopy for the mixtures given in Table 4.4. The 2P region corresponds to the two-phase region.

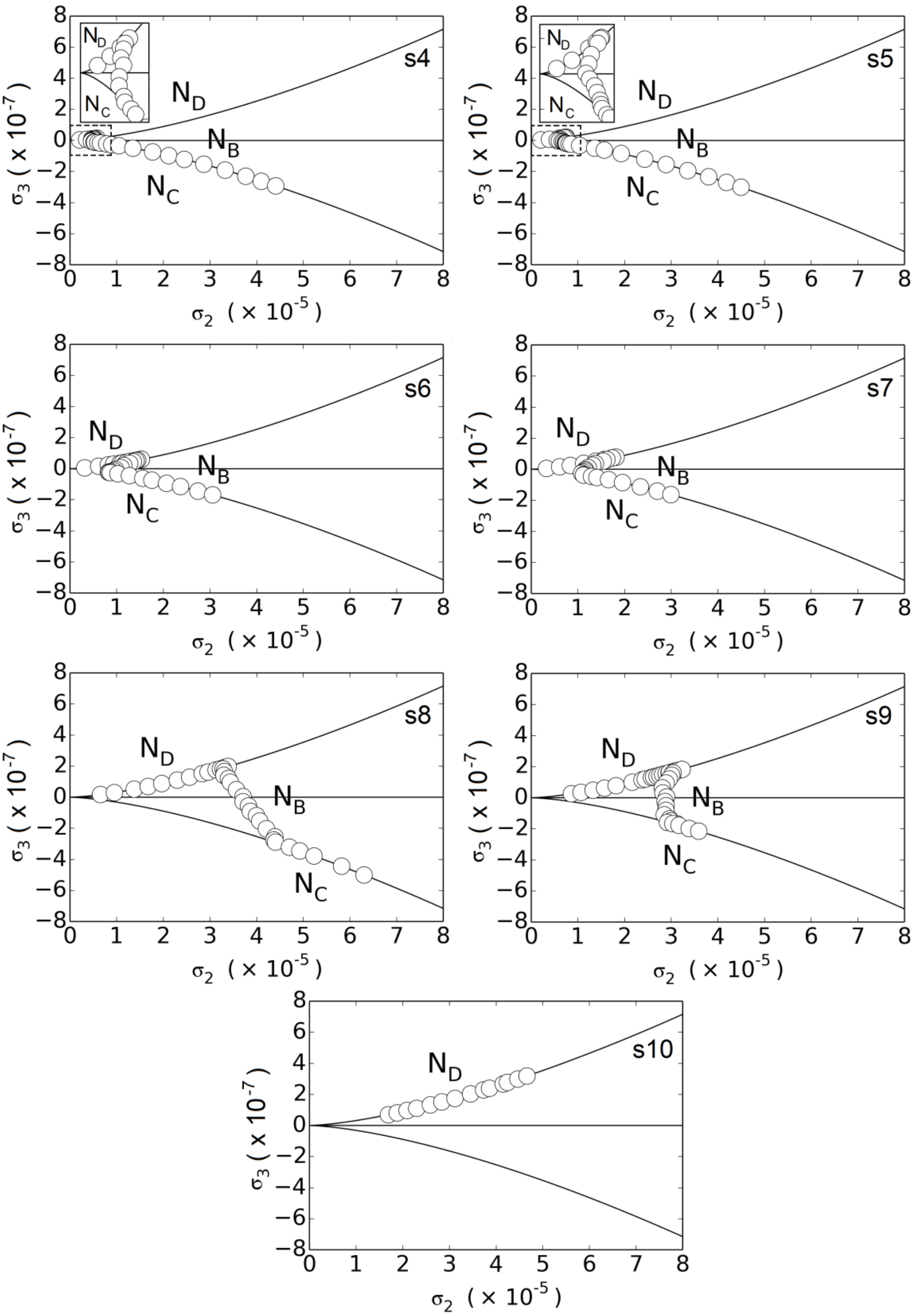

Figure 4.13. σ_3 versus σ_2 plots for the mixtures given in Table 4.4.

The SAXS curves analysis was performed in the framework proposed by Galerne et al. (Galerne et al., 1987) and Figueiredo et al. (Neto et al., 1985). The 2D SAXS patterns of our samples showed the same characteristics as theirs: the patterns' shape; the pseudo-lamellar structure in the three nematic phases; and the patterns' symmetry in the three aligned nematic phases, when the capillary is rotated to orientations (i) and (ii), as described in the Experimental section. Therefore, as in (Galerne et al., 1987; Neto et al., 1985) it is assumed the so-called intrinsic biaxial micelle, or IBM, model: the micelles have approximately the same average shape with an orthorhombic or biaxial symmetry in the three nematic phases; these micelles are stacked in blocks of just a few units in the three directions; the different nematic phases being triggered by changes in the orientational fluctuations of these micellar aggregates. In the uniaxial nematic phases, the orientational fluctuations are full rotations around the director, while in the biaxial nematic phase the orientational fluctuations are small amplitude oscillations around the directors.

As shown in (Galerne et al., 1987), the average dimensions A, B, C of the available volume per micelle can be obtained from $2\pi/q_x$, for X = A, B or C, where q_x is the band positions of the SAXS intensity curves as a function of q in the Axis 1 or 2 directions for dimensions A and B, and in the Axis 3 direction for C. The results for A, B and C for all the samples measured by SAXS are shown in Tables 4.1 and 4.2.

Once A, B and C were found, the average dimensions of the micelles A′, B′, C′ were calculated from a model that assumes the thickness of the layer around the micelle’s core is uniform as well as the density of the micelle’s core made of alkyl chains of the surfactant and cosurfactant molecules. Details of the model and its hypothesis as well as the calculations of the average polar layer thickness (w), of the micelles’ core average dimensions A′, B′, C′, of the average aggregation number (N_{agg}) and the average area per polar head (a_0) are given in the part 4.2. For some of the samples listed in Table 4.1, the results of the calculated parameters are shown in Table 4.5.

The shape anisotropy SA = {[(A′+B′)/2] – C′}/ [(A′+B′)/2] was also included in Table 4.5. It measures the average thickness of the micelle’s core bilayer C′ relative to the average of the other two dimensions A′ and B′ of the micelle’s core. The bilayer thickness is given by the lengths of the surfactant’s alkyl chain with very small variations due to temperature and composition of the mixture. Therefore, this shape anisotropy measures the relative growth of the micelle’s core in the directions perpendicular to the amphiphiles’ bilayer direction.

Table 4.5. Calculated parameters from SAXS measurements results for some samples listed in Table 3.2. Mixture identification, micelle's core average dimensions (A′, B′, C′), average polar layer thickness (w), average aggregation number (N_{agg}), average area per polar head (a_0), and shape anisotropy (*SA*).

Mixture	A′ (Å)	B′ (Å)	C′ (Å)	*w* (Å)	*SA*	N_{agg}	a_0 (Å^2)
s7	46.4 ± 2.4	35.0 ± 1.6	29.6 ± 1.4	14.4 ± 1.4	0.27 ± 0.04	150 ± 5	54 ± 4
s8	46.8 ± 1.5	35.1 ± 1.1	29.4 ± 0.9	14.4 ± 0.9	0.28 ± 0.03	150 ± 3	54 ± 2
s9	48.2 ± 1.7	35.7 ± 1.3	29.2 ± 1.1	14.4 ± 1.1	0.30 ± 0.03	156 ± 4	53 ± 3
s10	51.0 ± 2.6	36.2 ± 1.8	28.8 ± 1.5	14.8 ± 1.5	0.34 ± 0.04	166 ± 6	53 ± 4

4.4 Effect of the Sunset Yellow on the Stabilization of Lyotropic Nematic Phases

In the present study we concentrate on the effect of the SSY molecule in the lyotropic mixtures on the stabilization of different nematic phases, and, especially, on the biaxial nematic phase domain in the partial phase diagram. For this purpose, the mixtures given in Table 3.3 were prepared at different SSY concentrations. The results of laser conoscopy applied to these samples (Figures 4.14-4.17) are summarized in Table 4.6.

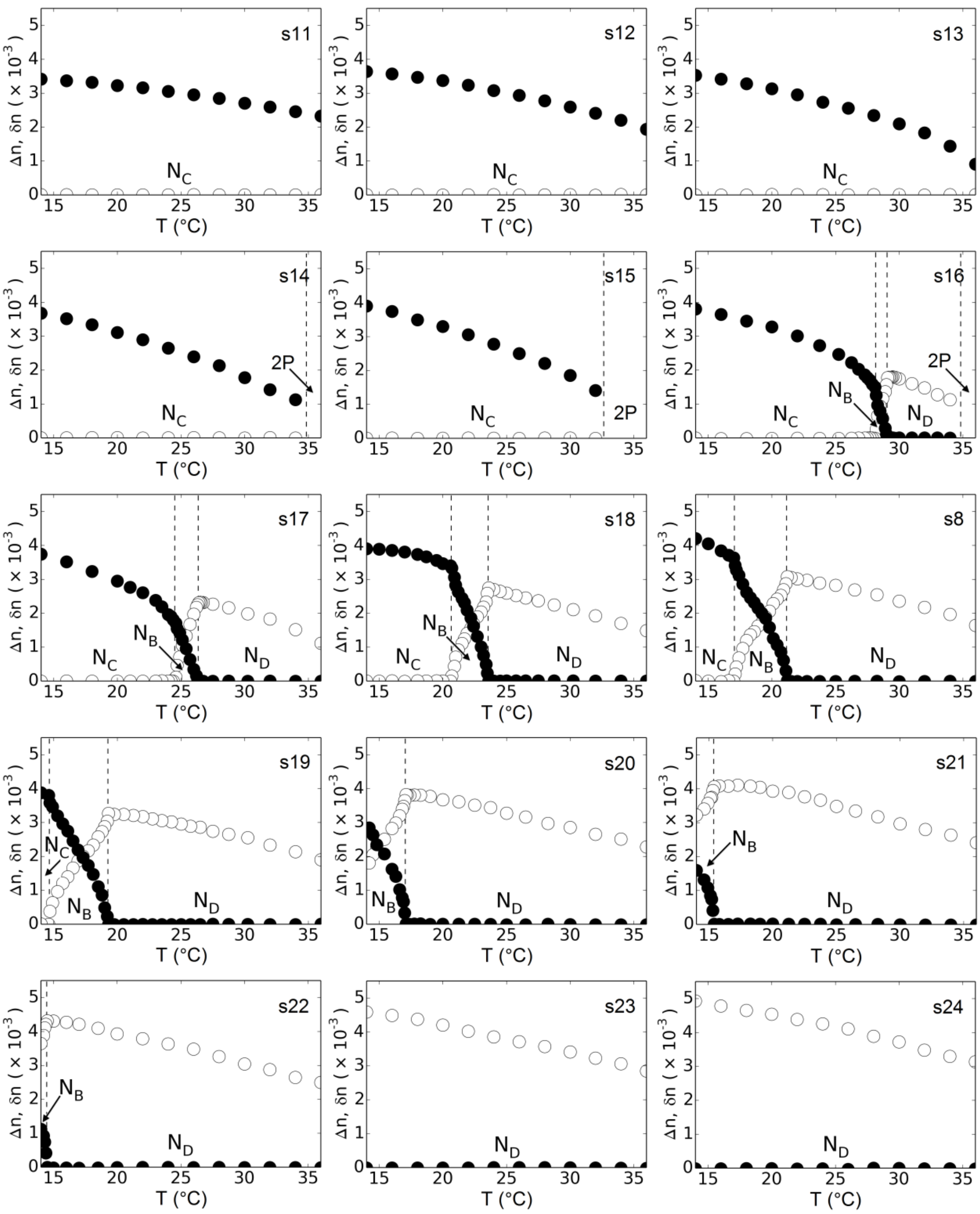

Figure 4.14. Birefringences as a function of temperature for lyotropic mixtures given in Table 4.6. The 2P region corresponds to the two-phase region. Δn (●) and δn (○).

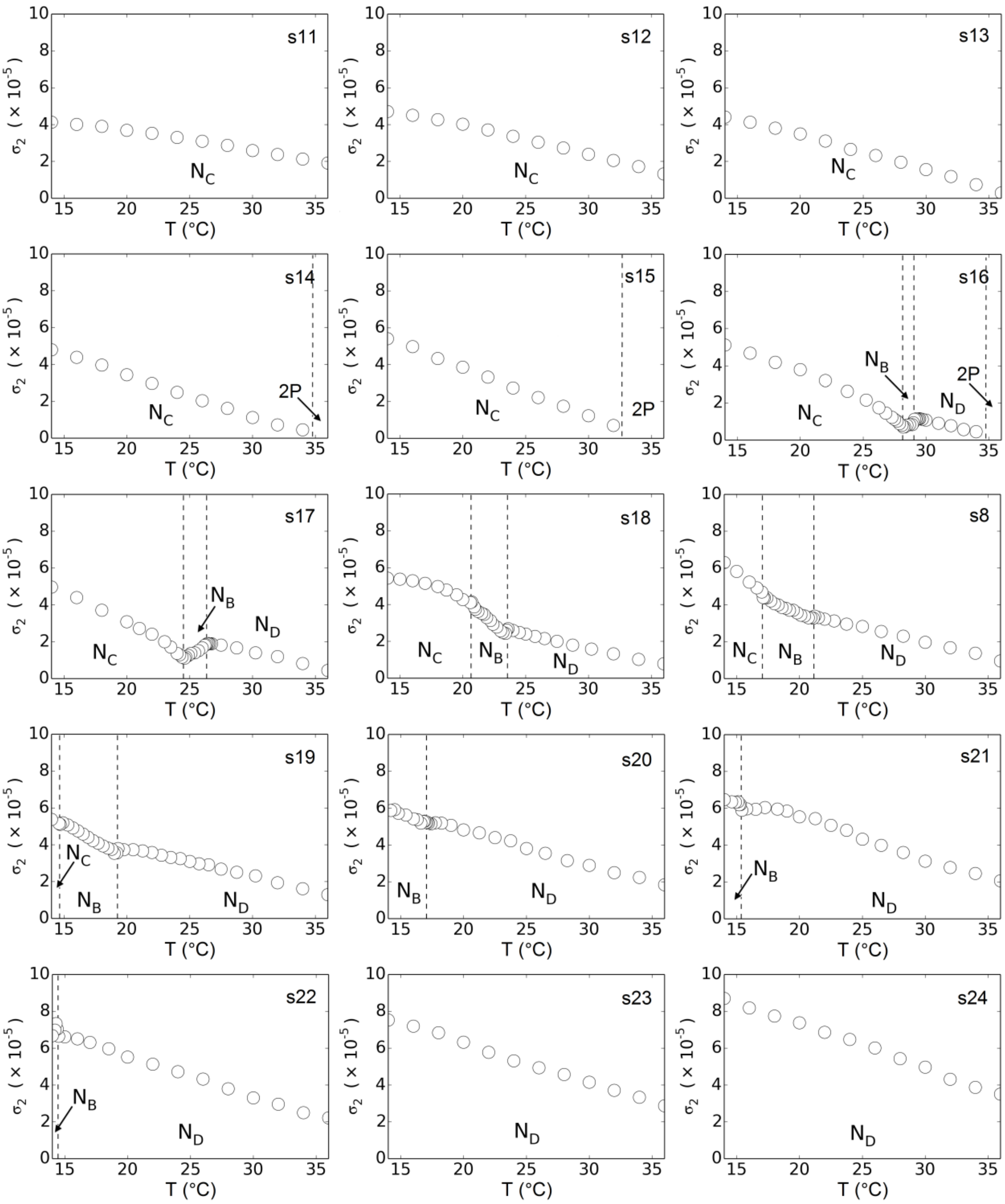

Figure 4.15. Temperature dependence of σ_2 values obtained from laser conoscopy for the mixtures given in Table 4.6. The 2P region corresponds to the two-phase region.

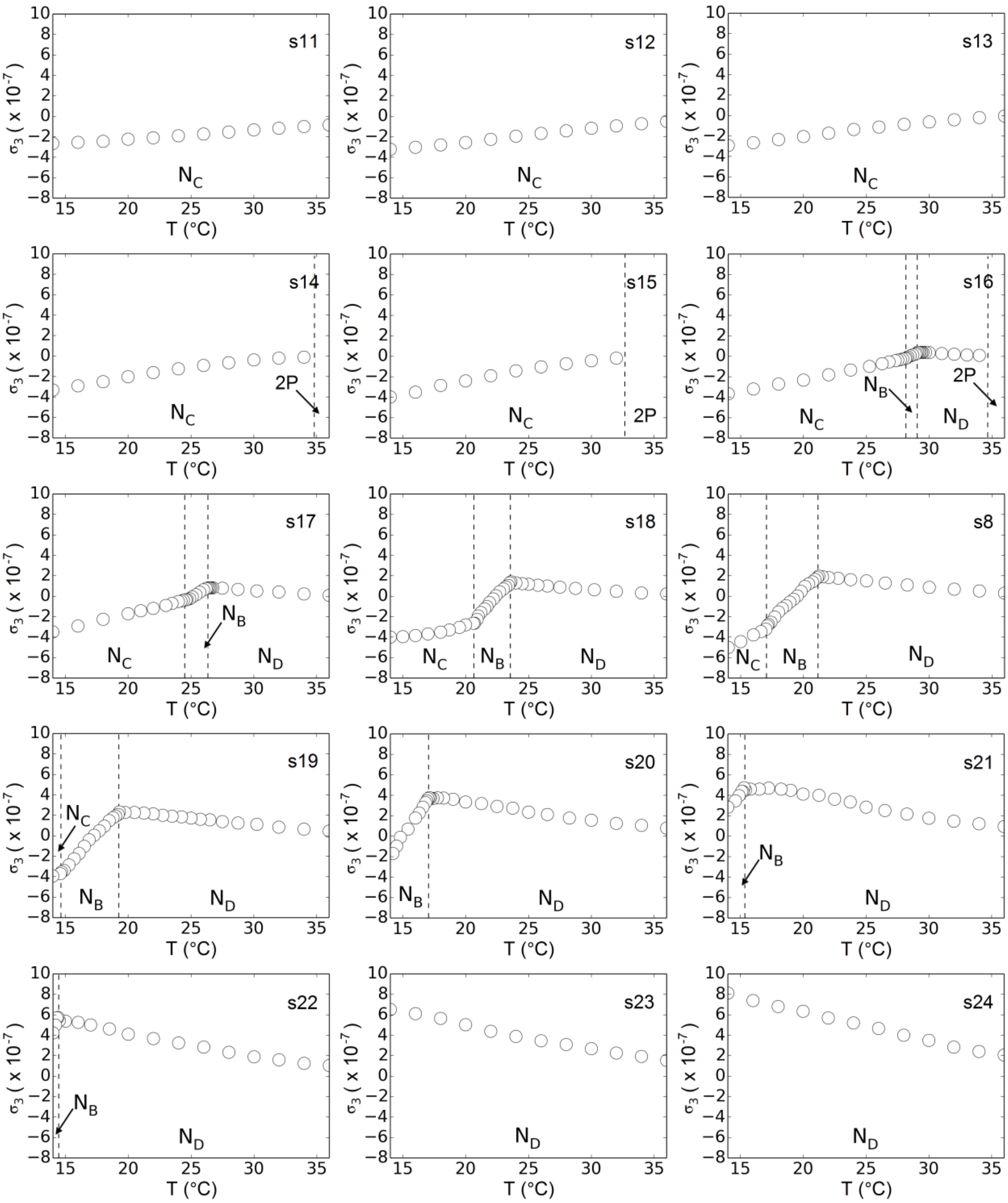

Figure 4.16. Temperature dependence of σ3 values obtained from laser conoscopy for the mixtures given in Table 4.6. The 2P region corresponds to the two-phase region.

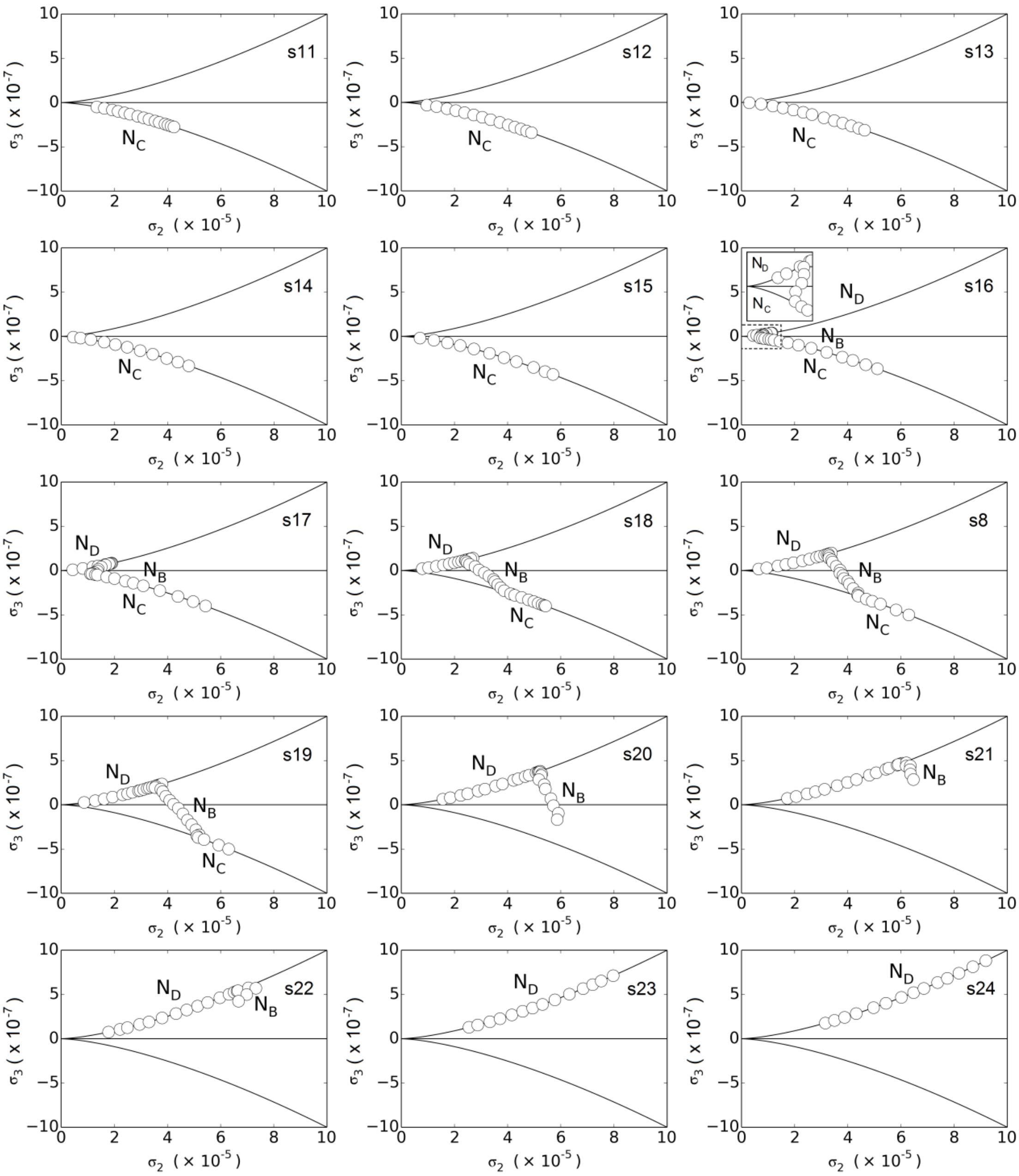

Figure 4.17. The dependence of σ_3 with σ_2 for the mixtures given in Table 4.6.

Table 4.6. Nematic-nematic transition temperatures, and temperature range of the biaxial nematic phase for the mixtures containing different concentrations of SSY, whose compositions were given in Table 3.3. Laser conoscopy measurements were done in the range from 14.0 ºC to 36.0ºC, so the phase transition temperatures are given considering the transitions in this temperature range.

Mixture	Phase transitions	ΔT_{N_B}/°C
s11	N_C	---
s12	N_C	---
s13	N_C	---
s14	$2P \xrightarrow{34.60°C} N_C$	---
s15	$2P \xrightarrow{32.20°C} N_C$	---
s16	$2P \xrightarrow{34.80°C} N_D \xrightarrow{29.05°C} N_B \xrightarrow{28.15°C} N_C$	0.90
s17	$N_D \xrightarrow{26.35°C} N_B \xrightarrow{24.50°C} N_C$	1.85
s18	$N_D \xrightarrow{23.65°C} N_B \xrightarrow{20.55°C} N_C$	2.90
s8	$N_D \xrightarrow{21.15°C} N_B \xrightarrow{17.05°C} N_C$	4.10
s19	$N_D \xrightarrow{19.25°C} N_B \xrightarrow{14.65°C} N_C$	4.60
s20	$N_D \xrightarrow{17.05°C} N_B$	---
s21	$N_D \xrightarrow{15.35°C} N_B$	---
s22	$N_D \xrightarrow{14.45°C} N_B$	---
s23	N_D	---
s24	N_D	---

In Table 4.6, the amount of SSY in the lyotropic mixture was increased from top to bottom. As can be seen, only the uniaxial N_C phase was obtained from the SSY-free mixture (s11) to the s15 mixture. Subsequently, there were mixtures with three phases (s8, and s16-s19), then mixtures with the transition from the N_B to a gel-type phase, without the transition to the N_C phase at low temperature (s20 and s22), and, finally, mixture with only the N_D phase (s23 and s24). As previously mentioned, the electrolyte ions added to the mixture bind to the surfactant head groups on the micelle surfaces by reducing the repulsions between the surfactant head groups (Rhein, 2007; Miqan et al., 2013), which causes the decrease in the micellar surface curvature (Myers, 2006), in order to go from the N_C phase domain to the N_D phase domain (Akpinar et al., 2016a). Considering the mixtures in Table 4.6, it is seen that the SSY molecule is effectively bound to the micelle surfaces, like the electrolyte ions, because as the concentration of the SSY increases in the mixtures, the N_D phase is more favorable. It should be noted that for mixtures s16 and 17, the samples (not completely but almost) lost the alignment around the N_{B-} to N_{B+} crossover, and when the samples entered the N_C phase region, they aligned again, giving the sharp interference pattern in the conoscopy experiment. This situation, named *anomalous behavior*, was already reported in one of our previous study for some DTMABr/NaBr/1-dodecanol/water mixtures (Akpinar et al., 2014). This behavior was attributed to the smaller micellar shape anisotropy according to their SAXS data. Then, the samples s16 and s17 realigned in the N_C phase region and the birefringences were measured until the N_{B-} to N_{B+} crossover by increasing temperature. The maximum values of the birefringences at the N_C-N_B phase transition for s16 and s17 are ~1.4x10^{-3} and ~1.8x10^{-3}, respectively. Then, for the samples s18, s8 and s19, those values are ~3.3x10^{-3}, ~3.5x10^{-3} and ~3.7x10^{-3}, respectively. As previously reported, there is a direct relation between the birefringences of the nematic phases and the micellar shape anisotropy: the higher (smaller) the birefringence, the higher (smaller) micellar shape anisotropy (Akpinar et al., 2012b; Akpinar et al., 2016a). Thus, the anomalous behavior, indicating the smaller micellar shape anisotropy in the biaxial phase, is observed at low SSY concentrations (s16 and s17). The further increase in the concentration of the SSY (s18, s8 and s19, respectively) causes both the increase in the micellar shape anisotropy and disappearance of the anomalous behavior.

One intriguing question present in the literature of the biaxial nematic mesophases is that this phase is stabilized only in small temperature-range domains. Therefore, it is important to obtain mixtures which give a wider biaxial phase region and to determine which factors extend the biaxial phase region. As it is known, the counterions are attached to the surfactant head groups on the surface of the micelles (in our case, negatively charged Br ions are the counterions of DTMABr surfactant molecule). In addition, to the mixtures obtained, researchers generally add inorganic salts, like NaBr, to the lyotropic mixtures if necessary. To determine the extent to which the SSY molecule enlarges the biaxial region by binding to the micelle surface, it would be appropriate to compare the mixtures of s4 and s1 prepared with the NaBr salt given in Table 3.1 with the mixtures of s8 (Table 3.2) and s20 (Table 3.3) having the same molar number and total mixture composition. Here, the mixture s4 has the same composition as the mixture s8 and the mixture s1 has the same composition as the mixture s20. The determined phase transition temperatures for the lyotropic nematic phases obtained from the s4 mixture containing NaBr are N_D-N_B: 30.05°C and N_B-N_C: 29.15°C. For the SSY-containing mixture of the same composition, those transition temperatures are 21.15°C and 17.05°C, respectively. When comparing biaxial phase regions, the biaxial nematic phase range for the s4 mixture is 0.90°C, while for s8 it is 4.10°C. A similar result was observed for mixtures s1 (~1.10°C) and s20 (~3.05°C), within the working-temperature range. As a result, when the SSY molecule is added to the mixtures with the same number of moles of NaBr, it is seen that the biaxial nematic phase region in the partial phase diagrams is about 4.5 times larger. This is one of the most important results of the present study, i.e. the dye molecule enlarges the biaxial phase range more with respect to the conventional salts. Furthermore, the increase in the concentration of the SSY molecule in the mixtures causes the enlargement of both N_D and N_B phase domains in the partial phase diagram (Figure 4.18).

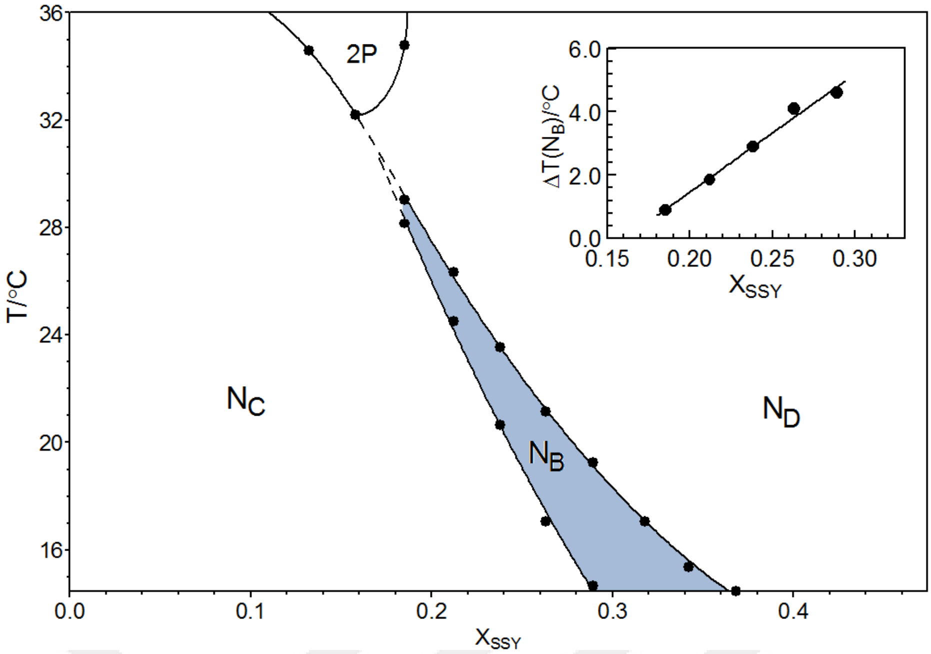

Figure 4.18. The partial phase diagram of the lyotropic mixtures given in Table 3.3 as a function of the concentration of the SSY. The inset shows the biaxial phase domain just for the mixtures presenting three nematic phases as a function of the temperature (s8 and s16-s19).

The effects of the increase of SSY concentration in the structure of the biaxial micelles for some of the mixtures of Tables 3.2 and 3.3 were also investigated by small angle X-ray scattering. As previously described, the structural parameters for the biaxial micelles were calculated from the SAXS results by a model assumption, the details of which are given in the part 4.2. Table 4.7 shows the results of the calculated parameters.

Table 4.7. Calculated parameters from SAXS measurements results for some samples listed in Table 3.2 and 3.3. Mixture identification, micelle's core average dimensions (A′, B′, C′), average polar layer thickness (w), average aggregation number (N_{agg}), average area per polar head (a_0), shape anisotropy (*SA*), and average number of SSY molecules per micelle (N_{SSY}). A′, B′, C′

Mixture	**A′ (Å)**	**B′ (Å)**	**C′ (Å)**	***w* (Å)**	***SA***	N_{agg}	a_0 (Å^2)	N_{SSY}
s8	46.8 ± 1.5	35.1 ± 1.1	29.4 ± 0.9	14.4 ± 0.9	0.28 ± 0.03	150 ± 3	54 ± 2	5.8 ± 0.1
s19	47.6 ± 1.9	35.7 ± 1.6	29.1 ± 1.3	14.6 ± 1.3	0.30 ± 0.04	154 ± 5	54 ± 3	6.6 ± 0.2
s20	48.5 ± 1.4	36.9 ± 1.1	28.9 ± 0.9	14.8 ± 0.9	0.32 ± 0.03	160 ± 4	53 ± 2	7.5 ± 0.2
s23	51.4 ± 1.7	39.6 ± 1.3	28.0 ± 1.1	15.3 ± 1.1	0.38 ± 0.03	177 ± 4	52 ± 2	11.1 ± 0.3

From Table 4.7, increasing the concentration of SSY in the host mixture increases the micelles' core dimensions A′ and B′ in the order of a few angstroms, but decreases the bilayer dimension C′ by a few sub-angstroms or keep it constant within the errors bars. This is better seen in the results of the *SA* parameter which measures the relative size of the bilayer dimension C′ with respect to the average of the other two perpendicular dimensions, A′ and B′. Figure 4.19 shows that increasing the SSY content of the mixture causes a growth of the micelles in the directions perpendicular to the micelle's bilayer at the working concentration range.

The other parameters calculated from the adopted model suggest that the micellar growth is accounted by the increase of the average aggregation number, while the average area per polar head of the surfactants is almost constant for all the mixtures. It means that the increase of SSY molecules in the mixtures induces more surfactant molecules to pack themselves in a single micelle, but the average area per surfactant molecule in the micelle's surface is almost the same for all the mixtures. While the molecules pack in a micelle, they do not stay nearer to each other, i.e., the micellar growth does not make the packing of molecules more compact. In addition, the *SA* parameter results showed that this increasing packing of molecules occurs on the sides of the micelles perpendicular to the bilayer.

Table 4.7 also shows that the increase in N_{agg} with the molar fraction of SSY is accompanied by the increase in the number of SSY molecules per micelle, N_{SYY}. This parameter was calculated from the ratio of the aggregation number to the molar ratio between the surfactants and the SSY molecules. Both the surfactant and cosurfactant molecules were included in the surfactants' moles number.

Comparisons of the results of Tables 4.5 and 4.7 for the C′ parameter of mixtures with different electrolytes or with SSY shows that the SSY molecules are not inside the micelles' core, but on the micelles' surface or in the water layer region. In both cases, the polar layer including the polar groups of the surfactants in the micelles' surfaces, the counter ions and the water around the micelles has an approximate size of 15 Å for all the mixtures, and therefore the largest surfaces of the plank-like SSY molecules have to be parallel or at most inclined to the biaxial micelles' faces, but not perpendicular to them due to geometrical reasons.

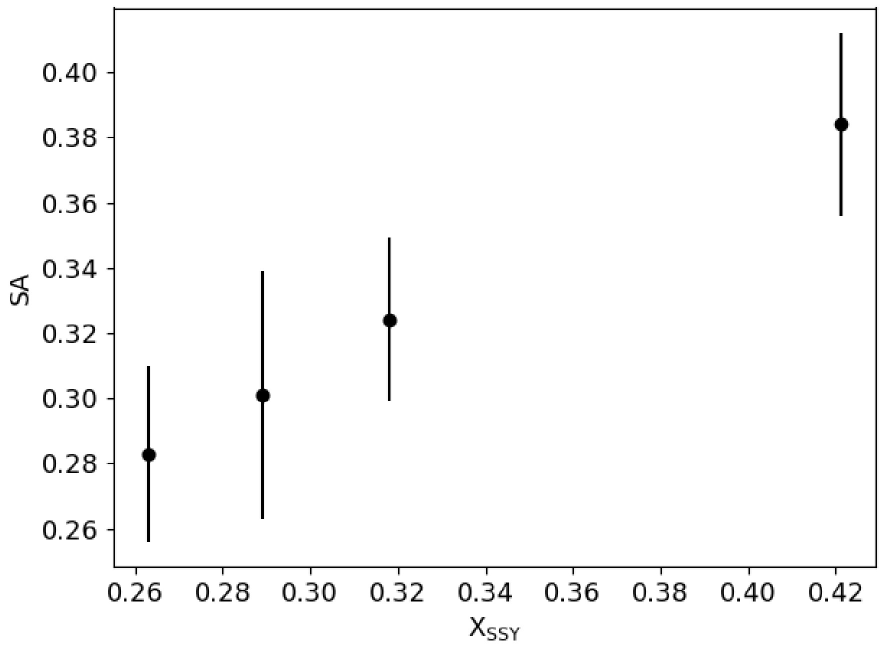

Figure 4.19. Shape anisotropy $SA = \frac{\frac{(A'+B')}{2} - C'}{\frac{(A'+B')}{2}}$ as a function of the molar percentage of sunset yellow for the mixtures listed in Table 4.7.

5. CONCLUSIONS

In this study, the presence of the Sunset Yellow dye molecule in the lyotropic mixtures was studied from the surfactant-dye interaction on the micelle surfaces point of view. Its effect was also compared with the conventional inorganic electrolytes in terms of the stabilization of the different lyotropic nematic phases and the biaxial phase domain in the partial phase diagrams. It was shown that Sunset Yellow exhibits a chaotropic character similar to the SCN^- ion, which is an important point to determine the degree of the interactions between the surfactant head groups and the anionic part of the Sunset Yellow on the micelle surfaces. The results indicated that Sunset Yellow interacts with the surfactant head groups effectively and it gives larger biaxial phase region in the partial phase diagrams with respect to the Hofmeister series anions of sodium salts. Furthermore, the degree of the binding of Sunset Yellow to the micelle surfaces causes the growth of the micellar shape anisotropy to mainly give the stabilization of N_D and/or N_B phase

6. REFERENCES

Akpinar E, Canioz C, Turkmen M, Reis D and Neto AMF (2018a) “Effect of the Surfactant Alkyl Chain Length on the Stabilisation of Lyotropic Nematic Phases”, Liquid Crystals, 45:2, 219–229

Akpinar E, Giesselmann F and Acimis M (2013) “Effect of Micelle Size and Intermicellar Distance on the Chirality Transfer in the Intrinsic Lyotropic Cholesteric Phases”, Liquid Crystals, 40:9, 1183-1194

Akpinar E, Guner E, Demir-Ordu O and Neto AMF (2019b) “Effect of Head-Group Size of Some Tetradecylalkylammonium Bromide Surfactants on Obtaining the Lyotropic Biaxial Nematic Phase”, Eur. Phys. J. E, 42, 44.

Akpinar E and Neto AMF (2019) “Experimental Conditions for the Stabilization of the Lyotropic Biaxial Nematic Mesophase”, Crystals, 9, 158.

Akpinar E, Otluoglu K, Turkmen M, Canioz C, Reis D and Neto AMF (2016b) “Effect of the Presence of Strong and Weak Electrolytes on the Existence of Uniaxial and Biaxial Nematic Phases in Lyotropic Mixtures”, Liq. Cryst., 43, 1693-1708.

Akpinar E, Reis D and Neto AMF (2014) “Anomalous Behavior in the Crossover Between the Negative and Positive Biaxial Nematic Mesophases in a Lyotropic Liquid Crystal”, ChemPhysChem, 15, 1463-1469.

Akpinar E, Reis D and Neto AMF (2012b) “Effect of Alkyl Chain Length of Alcohols on Nematic Uniaxial-to-Biaxial Phase Transitions in a Potassium Laurate/Alcohol/K_2SO_4/Water Lyotropic Mixture”, Liq. Cryst., 39, 881-888.

Akpinar E, Reis D and Neto AMF (2015) “Effect of Hofmeister Anions on the Existence of the Biaxial Nematic Phase in Lyotropic Mixtures of Dodecyltrimethylammonium Bromide/Sodium Salt/1-Dodecanol/Water”, Liq. Cryst., 42, 973-981.

Akpinar E, Reis D and Neto AMF (2012a) “Lyotropic Mixture Made of Potassium Laurate/1-Undecanol/K_2SO_4/Water Presenting High Birefringences and Large Biaxial Nematic Phase Domain: a Laser Conoscopy Study”, Eur. Phys. J. E, 35, 50

Akpinar E, Turkmen M, Canioz C and Neto AMF (2016a) “Role of Kosmotrope-Chaotrope Interactions at Micelle Surfaces on the Stabilization of Lyotropic Nematic Phases”, Eur. Phys. J. E, 39, 107.

Akpinar E, Uygur N, Uyanik S and Neto AMF (2019a) "Effect of Surfactant Alkyl Chain Length on Lyotropic Uniaxial to Biaxial Cholesteric Phase Transitions", Eur. Phys. J. E, 42: 128.

Akpinar E, Yurdakul S and Neto AMF (2018b) “Comparison between Lyotropic Cholesteric Phase Behavior with Partlyfluorinated Surfactants and Their Exact Hydrogenated Counterparts”, Journal of Molecular Liquids, 259 239–248

Alben R (1973) “Liquid Crystal Phase Transitions in Mixtures of Rodlike and Platelike Molecules”, J. Chem. Phys., 59, 4299-4304.

Alfutimie A, Curtis R and Tiddy GJT (2014) “Gel Phase (L_β) Formation by Mixed Saturated and Unsaturated Monoglycerides”, Colloids and Surfaces A: Physicochem. Eng. Aspects, 456 (2014) 286–295

Almeida MR, Stephani R, Dos Santos HF and Oliveira LFC (2010) "Spectroscopic and Theoretical Study of the “Azo”-Dye E124 in Condensate Phase: Evidence of a Dominant Hydrazo Form", J Phys Chem A, 114:526-34.

Ashiotis G, Deschildre A, Nawaz Z, Wright JP, Karkoulis D, Picca FE and Kieffer J (2015) “The Fast Azimuthal Integration Python Library: Pyfai”, J. Appl. Cryst., 48, 510-519.

Bartolino R, Chiaranza T, Meuti M and Compagnoni R (1982) “Uniaxial and Biaxial Lyotropic Nematic Liquid Crystals”, Phys. Rev. A, 26, 1116-1119.

Berejnov V, Raikher Y, Cabuil V, Bacri JC and Perzynski R (1998) "Synthesis of Stable Lyotropic Ferronematics with High Magnetic Content", Journal of Colloid and Interface Science, 199:215 – 217

Bilinov LM (2011) Structure and Physical Properties of Liquid Crystals, First Edition, Springer Press, Moscow.

Birdi KS (2014) Surface Chemistry Essentials, First edition, CRC Press, Boca Raton

Boden N, Corne S and Jolley K (1987) “Lyotropic Mesomorphism of the Cesium Pentadecafluorooctanoate/Water System: High-Resolution Phase Diagram”, J. Phys. Chem., 91, 4092-4105

Boden N, Radley K and Holmes MC (1981), "On the Relationship between the Micellar Structure and the Diamagnetic Anisotropy of Amphiphilic Nematic Mesophase", Mol. Phys., 42(2):493-496.

Braga WS, Kimura NM, Luders DD, Sampaio AR, Santoro PA and Palangana AJ (2007) “Reentrant Isotropic-Calamitic Nematic Phase Transition in Potassium Laurate-Decanol- D_2O Mixtures”, Eur. Phys. J. E, 24, 247-250.

Burducea G (2004) "Lyotropic Liquid Crystals Specific Structures", Romanian Reports in Physics, 56(1):66-86.

Buwalda RT and Engberts JBFN (2001) “Aggregation of Dicationic Surfactants with Methyl Orange in Aqueous Solution”, Langmuir, 17, 1054-1059.

Chakraborty T and Moulik SP (2005) “Micellization and Related Behavior of Binary and Ternary Surfactant Mixtures in Aqueous Medium: Cetyl Pyridinium Chloride (CPC), Cetyl Trimethyl Ammonium Bromide (CTAB) and Polyoxyethylene (10) Cetyl Ether (Brij-56) Derived System”, J Phys Chem B, 109, 2005, Pages 14813-14823.

Chami F and Wilson MR (2010) "Molecular Order in a Chromonic Liquid Crystal: A Molecular Simulation Study of The Anionic Azo Dye Sunset Yellow", J Am Chem Soc., 132:7794-802.

Chang CM and Bodmeier R (1997) "Effect of Dissolution Media and Additives on the Drug Release from Cubic Phase Delivery Systems", Journal of Controlled Released, 46(3):215-222.

Chen Y, Ma P and Gui S (2014) "Cubic and Hexagonal Liquid Crystals as Drug Delivery Systems", BioMed Research International, 2014:1-12.

Collings PJ, Asdonk PVD, Angel Martinez, Tortora L and Kouwer PHJ (2016) “Anchoring Strength Measurements of a Lyotropic Chromonic Liquid Crystal on Rubbed Polyimide Surfaces”, Liquid Crystals, 44:7, 1165-1172

Edwards DJ, Jones JW, Lozman O, Ormerod AP, Sintyureva M and Tiddy GJT (2008) “Chromonic Liquid Crystal Formation by Edicol Sunset Yellow”, J. Phys. Chem. B, 112, 14628-14636.

Edwards DJ, Ormerod A, Tiddy GJT, Jabber AA and Mahendrasingham A (1996) “Aggregation and Lyotropic Liquid Crystal Formation of Anionic Azo Dyes for Textile Fibres”, Adv. Color Chem. Ser., 4, 83-106.

Erdinc N and Gokturk S (2014) “Spectrophotometric and Conductometric Studies on the Interaction of Anionic Dye Eosin-Y with Cationic Micelles”, Analytical Chem. Lett., 4, 146-157.

Fairhurst CE, Fuller S, Gray J, M. Holmes MC and Tiddy GJT (1998) Lyotropic Surfactant Liquid Crystals in Handbook of Liquid Crystals, First Edition, Wiley, Weinheim

Fazeli S, Sohrabi B and Tehrani-Bagha AR (2012) “The Study of Sunset Yellow Anionic Dye Interaction with Gemini and Conventional Cationic Surfactants in Aqueous Solution”, Dyes and Pigments, 95, 768-775.

Filho AM, Laverde A and Fujiwara FY (2003) “Observation of Two Biaxial Nematic Mesophases in the Tetradecyltrimethylammonium Bromide/Decanol/Water System”, Langmuir, 19, 1127-1132.

Fong WK, Hanley T, Thiery B, Hawley A, Boyd B and Landersdorfer C (2016) "External Manipulation of Nanostructure in Photoresponsive Lipid Depot Matrix to Control and Predict Drug Release in Vivo", Journal of Controlled Release, 228:97-73.

Fontaini S, Barbero B and Neto AMF (1996) "Determination of the Effective Splay-Bend Elastic Constant of a Lyotropic Nematic Liquid Crystal", Phys. Rev. E, 53, 2454.

Fontell (1990) “Cubic Phases in Surfactant and Surfactant-Like Lipid Systems”, Colloid Polym Soi., 268:264-285

Freiser MJ (1970) “Ordered States of a Nematic Liquid”, Phys. Rev. Lett., 24, 1041-1043.

Freiser MJ (1971) “Successive Transitions in a Nematic Liquid”, Molecular Crystals and Liquid Crystals, 14:1-2, 165-182.

Galerne Y and Marcerou JP (1985) “Temperature-concentration behaviour of the order parameter in the nematic phases of a lyotropic liquid crystal”, J. Physique France, 46, 589-594.

Galerne Y, Neto AMF and Liébert L (1987) “Microscopical Structure of the Uniaxial and Biaxial Lyotropic Nematics”, J. Chem. Phys., 87, 1851-1856.

Garti N and Aserin A (2012) Micelles and Microemusions as Food Ingredient and Nutraceutical Delivery Systems, First Edition, Woodhead Publishing, Elsevier science and technology, Cambridge

Geelhaar T, Griesar K and Reckmann B (2013) “125 Years of Liquid Crystals—A Scientific Revolution in The Home”, Angew. Chem. Int. Ed., 52, 8798 – 8809

Gennes PG (1974) The Physics of Liquid Crystals, Second Edition, Clarendon Press, Oxford

Gohain B and Dutta RK (2008) "Premicellar and Micelle Formation Behavior of Dye Surfactant Ion Pairs in Aqueous Solutions: Deprotonation of Dye in Ion Pair Micelles", J Colloid Interf Sci., 323:395-402.

Gokturk S and Tuncay M (2003a) "Spectral Studies of Safranin-O in Different Surfactant Solutions", Spectrochimica Acta A, 59 (2003) 1857–1866.

Gokturk S and Tuncay M (2003b) “Dye-Surfactant Interaction in the Premicellar Region”, J. Surf. Deterg., 6, 325-330.

Halperin BI and Nelson DR (1978) “Theory of Two-Dimensional Melting”, Phys. Rev. Lett., 41.121-124

Heakal F.E. and Elkholy A.E. (2017) “Gemini Surfactants as Corrosion Inhibitors for Carbon Steel”, Journal of Molecular Liquids, 230 395-407

Ho CC, Goets RJ and El-Aasser MS (1981) “A Biaxial Lyotropic Nematic Phase in Dilute Solutions of Sodium Lauryl Sulfate-1-Hexadecanol-Water”, Langmuir, 7, 630-635.

Horowitz VR, Janowitz LA, Modic AL, Heiney PA and Collings PJ (2005) “Aggregation Behavior and Chromonic Liquid Crystal Properties of an Anionic Monoazo Dye”, Phys. Rev. E, 72, 041710.

Ibrhim OA, Al-Tikrity E, Latif IAA and Salih HK (2017) “Study the Effect of Adding Silver Nanoparticles on the Electrical Properties of the Binary System Mixture of Compounds with Liquid Crystal Properties”, Tikrit Journal of Pure Science 22 (2) 1813 – 1662.

Ishihara S and Mizusaki M (2019) “Alignment Control Technology of Liquid Crystal Molecules”, J Soc Inf Display, 2020;28:44–74.

Jennings KH, Marshall ICB, Wilkinson MJ, Kremer A, Kirby AJ and Camilleri P (2002) "Aggregation Properties of a Novel Class of Cationic Gemini Surfactants Correlate with Their Efficiency as Gene Transfection Agents", Langmuir, 18:2426-9

Joshi L, Kang S, Agra-Kooijman DM and Kumar S (2009) “Concentration, Temperature, and Ph Dependence of Sunset-Yellow Aggregates in Aqueous Solutions: An X-Ray Investigation”, Phys. Rev. E, 80, 041703.

Kale KM and Zana R (1977) “Effect of the Nature of the Counterion on the Volume Change upon Micellization of Ionic Detergents in Aqueous Solutions”, Journal of Colloid and Interface Science, Vol. 61. No. 2

Khan NM and Sarwar A (2006) “Study of Dye–Surfactant Interaction: Aggregation and Dissolution of Yellowish in N-Dodecyl Pyridinum Chloride”, Fluid Phase Equilibria, 239, 166-171.

Kim Y, Cukrov G, Vita F, Scharrer E, Samulski ET, Francescangeli O and Lavrentovich OD (2016) “Search for Microscopic and Macroscopic Biaxiality in the Cybotactic Nematic Phase of New Oxadiazole Bent-Core Mesogens”, Phys. Rev. E, 93, 062701.

Kim Y, Senyuk B, Shin S, Kohlmeier A, Mehl GH and Lavrentovich OD (2014) “Surface Alignment, Anchoring Transitions, Optical Properties, and Topological Defects in the Thermotropic Nematic Phase of Organo-Siloxane Tetrapodes”, Soft Matter, 10, 500-509.

Kirby JA, Camilleri P, Engberts JBFN, Feiters MC, Nolte RJM, Soderman O, Bergsma M, Bell P, Fielden ML, Rodríguez CLG, Guédat P, Kremer A, McGregor C, Perrin C, Ronsin G and Eijk MCPV (2003) "Gemini Surfactants: New Symthetic Vectors for Gene Transfection", Angew. Chem. Int. Ed., 42, 1448 – 1457

Knudsen EB, Sørensen HO, Wright JP, Goret G and Kieffer J (2013) “Fabio: Easy Access to Two-Dimensional X-Ray Detector Images in Python”, J. Appl. Cryst., 46, 537-539

Kroin T and Neto AMF (1987) "Bend Periodic Distortion of the Texture in Nematic Lyotropic Liquid Crystals with and without Ferrofluid", Phys. Rev. A, 36, 2987.

Kumar B, Tikariha D and Ghosh KK (2012) “Effects of Electrolytes on Micellar and Surface Properties of Some Monomeric Surfactants”, J. Disp. Sci. Technol, 33, 265-271.

Lawson KD and Flautt TJ (1967) "Magnetically Oriented Lyotropic Luquid Crystalline Phases", J.Am. Chem. Soc, 89, 5489.

Lenglet J, Bourdon A, Bacri JC and Demoucy G (2002) “Thermodiffusion in Magnetic Colloids Evidenced and Studied by Forced Rayleigh Scattering Experiments”, Phys. Rev. E, 65, 031408-1-14.

Leontidis E (2002) “Hofmeister Anion Effects on Surfactant Self-Assembly and the Formation of Mesoporous Solids”, Curr. Opin. Colloid Interface Sci., 7, 81-91.

Lombardo D, Kiselev MA, Magazù S and Calandra P (2015) "Amphiphiles Self-Assembly: Basic Concepts and Futureperspectives of Supramolecular Approaches", Advances in Condensed Matter PhysicsVolume, 10.1155-151683,22

Luckhurst GR and Sluckin TJ (2015) Biaxial Nematic Liquid Crystals: Theory, Simulation and Experiment, First Edition, Wiley, Chishester

Lydon J (2010) “Chromonic Review”, J. Mater. Chem., 20, 10071-10099.

Lydon J (2011) "Chromonic Liquid Crystalline Phases", Liquid Crystals, Vol. 38, Nos. 11–12, 1663–1681.

Madsen LA, Dingemans TJ, Nakata M and Samulski ET (2004) “Thermotropic Biaxial Nematic Liquid Crystals”, Phys. Rev. Lett., 92, 145505.

Marcus Y (2009) “Effect of Ions on the Structure of Water: Structure Making and Breaking”, Chem. Rev., 109, 1346-1370.

Miqan SN, Tabrizi FF, Abedini H and Kashi HA (2013) “Estimation of Micellization Parameters ff Sds in the Presence of Some Electrolytes for Emulsion Polymerization Systems”, J. Surfact. Deterg., 16, 271-278.

Myers D (2006) Surfactant Science and Technology, Third Edition, John Wiley & Sons, New Jersey.

Nasrin L, Kabir E and Rahman M (2016) “External Magnetic Field-Dependent Tricritical Points of Uniaxial-to-Biaxial Nematic Transition”, Phase Trans., 89, 193-201.

Nehalatha M, Sekar N, Jayakumar VS and Joe H (2008) "Quantum Chemical Computations and Fourier Transform Infrared Spectral Studies of a Nonlinear Food Dye E110", Spectrochim Acta A, 69:82-90.

Nehring YJ and Saup A (1972) “On the Schlieren Texture in Nematic and Smectic Liquid Crystals”, Chem. Soc., 2, 68, 1-15

Neto AMF (2014) “Micellar Cholesteric Lyotropic Liquid Crystals”, Liquid Crystals Reviews, 2:1, 47-59

Neto AMF, Galerne Y, Levelut AM and Liébert L (1985) “Pseudo-Lamellar Ordering in Uniaxial and Biaxial Lyotropic Nematics: A Synchrotron X-Ray Diffraction Experiment”, J. Physique Lett., 46, 499-505.

Neto AMF and Salinas SRA (2005) The Physics of Lyotropic Liquid Crystals: Phase Transitions and Structural Properties, First Edition, Oxford University Press, New York.

Nicolettat FP, Chidishimo G, Golemme A and Picci N (1991) “Phases and Phase Transitions in a Nematic Lyotropic System with a Biaxial Phase”, Liq. Cryst., 10, 665-674.

Oliveira EA, Liebert L and Neto AMF (1989) “A New Soap/Detergent/Water Lyotropic Liquid Crystal with a Biaxial Nematic Phase”, Liq. Cryst., 5, 1669-1675.

Oliveira SR (2006) Interação de Ácido Algínico com Surfactantes Catiônicos em Solução Aquosa, Doctoral thesis, Universidade Estadual Paulista, Júlio de Mesquita Filho, São José do Rio Preto

Oliveira EA, Barbero G and Neto AMF (1996) "Metastable Periodic Freedericksz Transition in Nematic Liquid Crystals", Phys. Rev. E, 54, 5830.

Panizza M, Delucchi M and Cerisola G (2005) “Electrochemical Degradation of Anionic Surfactants”, Journal of Applied Electrochemistry, 35:357–361.

Park H, Kang S, Tortora L, Nastishin Y, Finotello D, Kumar S and Lavrentovich OD (2008) “Self-Assembly of Lyotropic Chromonic Liquid Crystal Sunset Yellow and Effects of Ionic Additives”, J. Phys. Chem. B, 112, 16307-16319.

Quist P (1995) “First Order Transitions to a Lyotropic Biaxial Nematic”, Liquid Crystals, 18:4, 623-629

Renshaw MP and Day IJ (2010) "NMR Characterization of the Aggregation State of the Azo Dye Sunset Yellow in the Isotropic Phase" J Phys Chem B, 114: 10032-8.

Rhein L (2007) “Surfactant Action on Skin and Hair: Cleansing and Skin Reactivity Mechanisms”, Handbook for Cleaning/Decontamination of Surfaces, 1, 305-369.

Rizwan SB, Boyd BJ, Rades T and Hook S (2010) “Bicontinuous Cubic Liquid Crystals as Sustained Delivery Systems for Peptides and Proteins”, Expert Opin. Drug Deliv., 7(10)

Senyuk B “Liquid Crystals: A Simple View on a Complex Matter”, http://www.personal.kent.edu/~bisenyuk/liquidcrystals/maintypes2.html, July 4, 2020

Shah JC, Sadhale Y and Chilukuri DM (2001) "Cubic Phase Gels as Drug Delivery Systems", Advanced Drug Delivery Reviews, 47(2-3):229-250.

Shahir AA, Javadian S, Razavizadeh M and Gharibi H (2011) “Comprehensive Study of Tartrazine/Cationic Surfactant Interaction”, J. Phys. Chem. B, 115, 14435-14444.

Simoes M, Pazetti M, Kimura NM and Palangana AJ (2010) “Micellar Shape Anisotropy on Lyotropic Nematic Phases”, Physica A, 389, 4000-4008.

Simoncic B and Kovac F (1998) “A Study of Dye-Surfactant Interactions. Part 2. The Effect of Purity of a Commercial Cationic Azo Dye on Dye-Surfactant Complex Formation”, Dyes and Pigments, 40, 1-9.

Singh S (2002) Liquid Crystal Fundementals, First Edition, Word Scientific Press, New Jersey

Sohrabi B, Bazyari A and Hashemianzadeh M (2010) "Effect of Ethylene Glycol on Micellization and Surface Properties of Gemini Surfactant Solutions", Colloid Surf A, 364:87-93.

Tam-Chang SW and Huang L (2008) "Chromonic Liquid Crystals: Properties and Applications as Functional Materials" Chem. Commun., 1957–1967

Tidy JT, Mateer DL, Ormerod AP, Harrison WJ and Edwards DJ (1995) "Highly Ordered Aggregates in Dilute Dye-Water Systems", Langmuir, 1995,11, 390—393

Tanford C (1980) The Hydrophobic Effect, John Wiley and Sons, New York.

Tresset G (2009) “The Multiple Faces of Self-Assembled Lipidic Systems”, PMC Biophysics, 10.1186/1757-5036-2-3

Tunc S and Duman O (2007) "Investigation of Interactions between Some Anionic Dyes and Cationic Surfactants by Conductometric Method", Fluid Phase Equilibria, 251 (2007) 1–7

Umapathi R, Reddy PM, Rani A and Venkatesu P (2018) “Influence of Additives on Thermoresponsive Polymers in Aqueous Media: A Case Study of Poly(N-Isopropylacrylamide”, Phys. Chem. Chem. Phys., 20, 9717-9744.

Vasilevskaya AS, Kitaeva EL and Sonin AS (1990) “Optically Biaxial Mesophases in Lyotropic Nematics”, Russ. J. Phys. Chem., 64, 599–601.

Wen J, Shen X, Shen H and Zhang FS (2014) “Hofmeister Series and Ionic Effects of Alkali Metal Ions on DNA Conformation Transition in Normal and Less Polarised Water Solvent”, Mol. Phys., 112, 2707-2719.

Wolff T and Klaussner B (1995) “Overlap of Colloid Chemistry and Photochemistry in Surfactant Systems”, Adv. Colloid Interface Sci., 59, 31-94.

Yang J (2004) "Interaction of Surfactants and Aminoindophenol Dye", J. Colloid Interface Sci., 274 237–243.

Yu LJ and Saupe A (1980) “Observation of a Biaxial Nematic Phase in Potassium Laurate-1-Decanol-Water Mixtures”, Phys. Rev. Lett., 45, 1000-1003.

Yu LJ and Saupe A (1982) “Deuteron Resonance of D_2O of Nematic Disodium Cromoglycate-Water Systems”, Mol. Cryst. Liq. Cryst., 80, 129-134.

Zhang G, Zhai X, Liu M, Tang Y and Zhang Y (2007) "Regulation of Aggregation and Morphology of Cyanine Dyes on Monolayers via Gemini Amphiphiles", J Phys. Chem B, 111:9301-8.

7. CURRICULUM VITAE

Name SURNAME **:** Gökhan TOPÇU

Place and Date of Birth :

Universities :

Bachelor's Degree :

e-mail :

Address :

List of Publications :

Hobbies :